# 12
# BEHAVIOUR OF SEDIMENT AFTER CAPITAL DISPOSAL

# LYTTELTON HARBOUR/WHAKARAUPŌ CHANNEL DEEPENING PROJECT

# Numerical modelling of sediment dynamics for a proposed offshore disposal ground

Prepared for Lyttelton Port of Christchurch

*PO Box 441, New Plymouth, New Zealand*
*T: 64-6-7585035 E: enquiries@metocean.co.nz*

MetOcean Solutions Ltd: P0201-01

March 2016

Report status

| Version | Date | Status | Approved by |
|---|---|---|---|
| RevA | 25/03/2016 | Draft for internal review | Weppe |
| RevB | 29/03/2016 | Draft for internal review | Beamsley |
| RevC | 30/03/2016 | Updated draft for internal review | Weppe |
| RevD | 31/03/2016 | Draft for client review | McComb |
| RevE | 19/05/2016 | Draft following client review | Beamsley |
| RevF | 19/05/2016 | Updated draft following client review | Beamsley |
| Rev0 | 21/09/2016 | Approved for release | Beamsley |
| | | | |
| | | | |
| | | | |

It is the responsibility of the reader to verify the currency of the version number of this report.



*PO Box 441, New Plymouth, New Zealand*
*T: 64-6-7585035 E: enquiries@metocean.co.nz*

**TABLE OF CONTENTS**

**LIST OF FIGURES**

**LIST OF TABLES**

# 1. INTRODUCTION

Lyttelton Port Company Limited (LPC) proposes deepening of the harbour shipping channel and turning basin to accommodate vessels with increased draughts, and disposing of the dredged material at an offshore site. A full description of the Channel Deepening Project (CDP) activities, location and methodologies is provided in Section Two (Project Description) of the associated Assessment of Environmental Effects (AEE), while Figure 1. provides an outline of the proposed deepened channel and capital disposal ground. The estimated volume to be dredged is of the order 18 M $m^3$ (including channel and berth pocket deepening, and reclamation construction); intended to be spread between 2 dredging campaigns; each taking between 9-14 months, with sediment disposed of at a 2.5x5.0 km proposed capital dredging disposal site situated approximately 6 km from Godley Head (Figure 1.1).

LPC have commissioned MetOcean Solutions Ltd (MSL) to undertake a numerical model study to investigate the morphological effects and associated sediment transport patterns associated with the disposal of capital dredged material at the proposed offshore disposal site and the effects of the mound on the offshore wave height gradient (Figure 1.1) Within the marine environment, morphological changes are a function of the salient sediment entrainment and transport mechanism, i.e. waves, tidal and residual currents. Numerical models are useful tools to examine these processes, especially where complex sediment dynamics arise from strong spatial energy gradients such as at the proposed disposal site; situated in the lee of Banks Peninsula and offshore from the Lyttelton Harbour tidal inlet.

This study applies a coupled wave, current and morphological model system (Delft3D) to examine expected patterns of long term morphological changes as well as extreme event time-domain simulations of actual historical events. Examining these energetic events provides insights into the salient processes responsible for the most significant morphological changes to the environs, and the characteristics of these expected morphological changes. The coupled modelling system is placed within broader regional wave and 3D hydrodynamic models of the environs (SWAN and ROMS respectively). These regional wave and hydrodynamics were calibrated using field measurements of wave and flow within Pegasus Bay. However, given the limited empirical information on underlying sediment texture and historical morphological behaviour, the sediment transport and morphology models were not specifically calibrated and validated. Accordingly the sediment transport and morphology models are used here as tools to understand the governing processes and to identify the qualitative patterns of morphological changes and key pathways of transport. As such, relative changes in morphology provide guidance on how sediment discharged of at the disposal site can be expected to move within the offshore environment.

This report is structured as follows. Section 2 details the methodologies used; including bathymetry sources, regional hindcast wave modelling (inclusive of validation), regional and local scale hydrodynamic modelling (inclusive of validation) and the sediment dynamic modelling methodology. Sensitivity testing of the user defined Erosion parameter is detailed in Section 3, while Section 4 details the specific morphological modelling techniques and parameters used, including the derived input reduction forcing conditions and

specific time-domain simulations. Morphological results are presented in Section 4 and a summary is provided in Section 5. References are cited in sections 6.

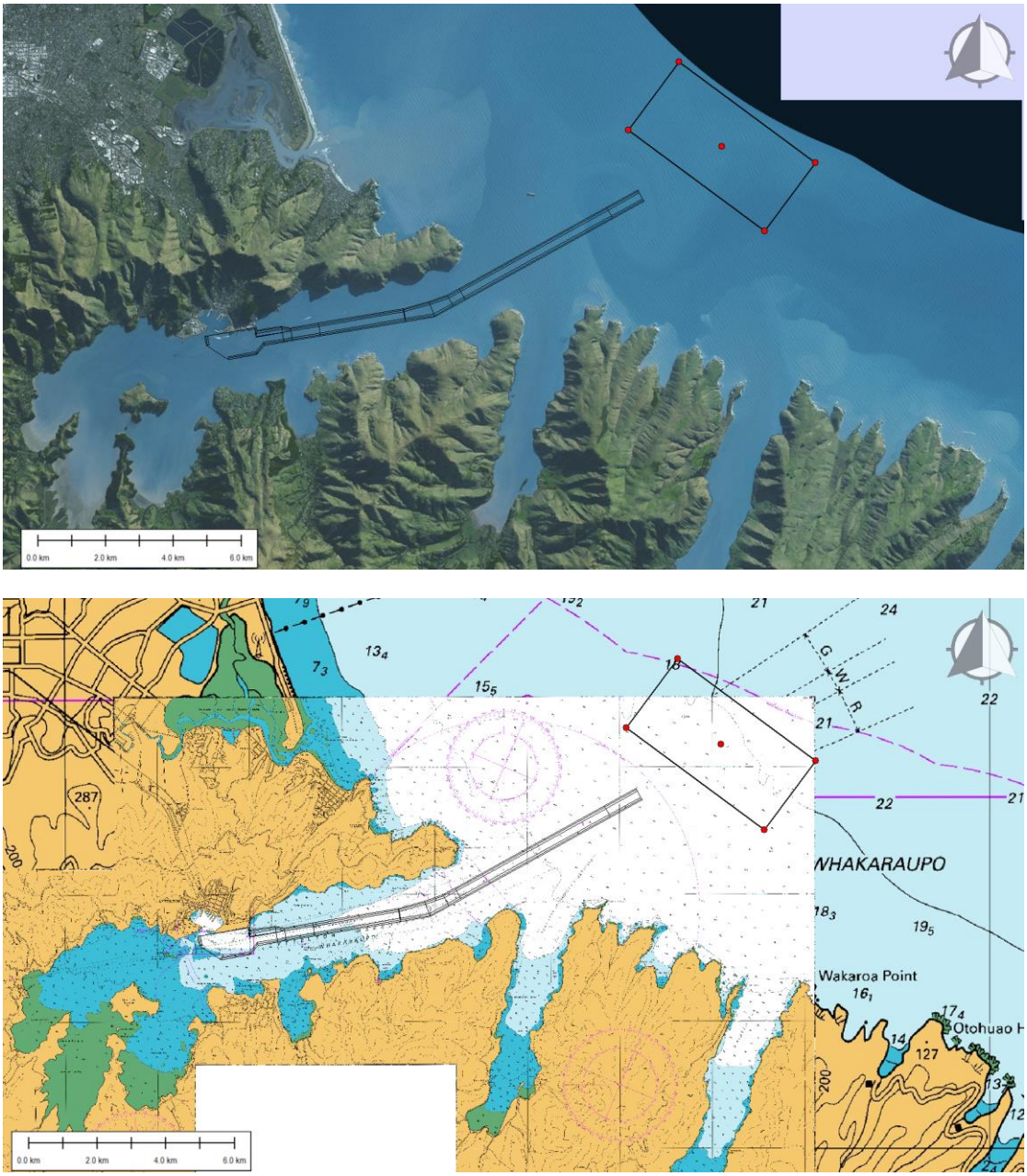


Figure 1.1 The location of the proposed deepened shipping channel and offshore capital dredging disposal ground against aerial image (top) and navigation charts (bottom).

# 2. METHODS

## 2.1. Bathymetry

Bathymetry data was obtained from a variety of sources including the regional electronic navigation charts (ENCs) from Land Information New Zealand (LINZ) and multibeam surveys within the main channel of Lyttelton harbour supplied by LPC.

## 2.2. Wave modelling methods

### 2.2.1. Numerical model

SWAN (Simulating Waves Nearshore) was used to prepare a 10-year wave hindcast (2003-2012). SWAN is a third generation ocean wave propagation model, which solves the spectral action density balance equation for wavenumber-direction spectra. This means that the growth, refraction, and decay of each component of the complete sea state, each with a specific frequency and direction, is solved, giving a complete and realistic description of the wave field as it changes in time and space. A detailed description of the model equations, parameterizations, and numerical schemes can be found in Holthuijsen, (2007) or the SWAN documentation[1]. Physical processes that are simulated include the generation of waves by surface wind, dissipation by white-capping, resonant nonlinear interaction between the wave components, bottom friction and depth limited breaking. All 3$^{rd}$ generation physics are included. The Collins (1972) friction scheme is used for wave dissipation by bottom friction with a friction factor of 0.015. The solution of the wave field is found for the non-stationary (time-stepping) mode. Boundary conditions, wind forcing and resulting solutions are all time dependent, allowing the model to capture the growth, development and decay of the wave field.

### 2.2.2. Model domain and boundary conditions

The wave hindcast involved a three-level SWAN downscaling, with full spectral boundaries for the lower-resolution domain prescribed from MetOcean Solutions implementation of the global wave model WW3 (Tolman, 1991). The Outer SWAN domain covered all New Zealand at resolution of 0.05˚ by 0.05˚; providing spectral boundaries to an intermediate SWAN nest, extending around the Banks Peninsula at 0.005˚ by 0.0038˚ resolution. The Lyttelton Harbour was modelled using a high-resolution (0.0008˚ by 0.0005˚) SWAN domain, nested within the Banks Peninsula domain. The model depths and example snapshots for the Lyttelton high-resolution domain are shown in Figure 2.1

[1] http://swanmodel.sourceforge.net/online_doc/online_doc.htm

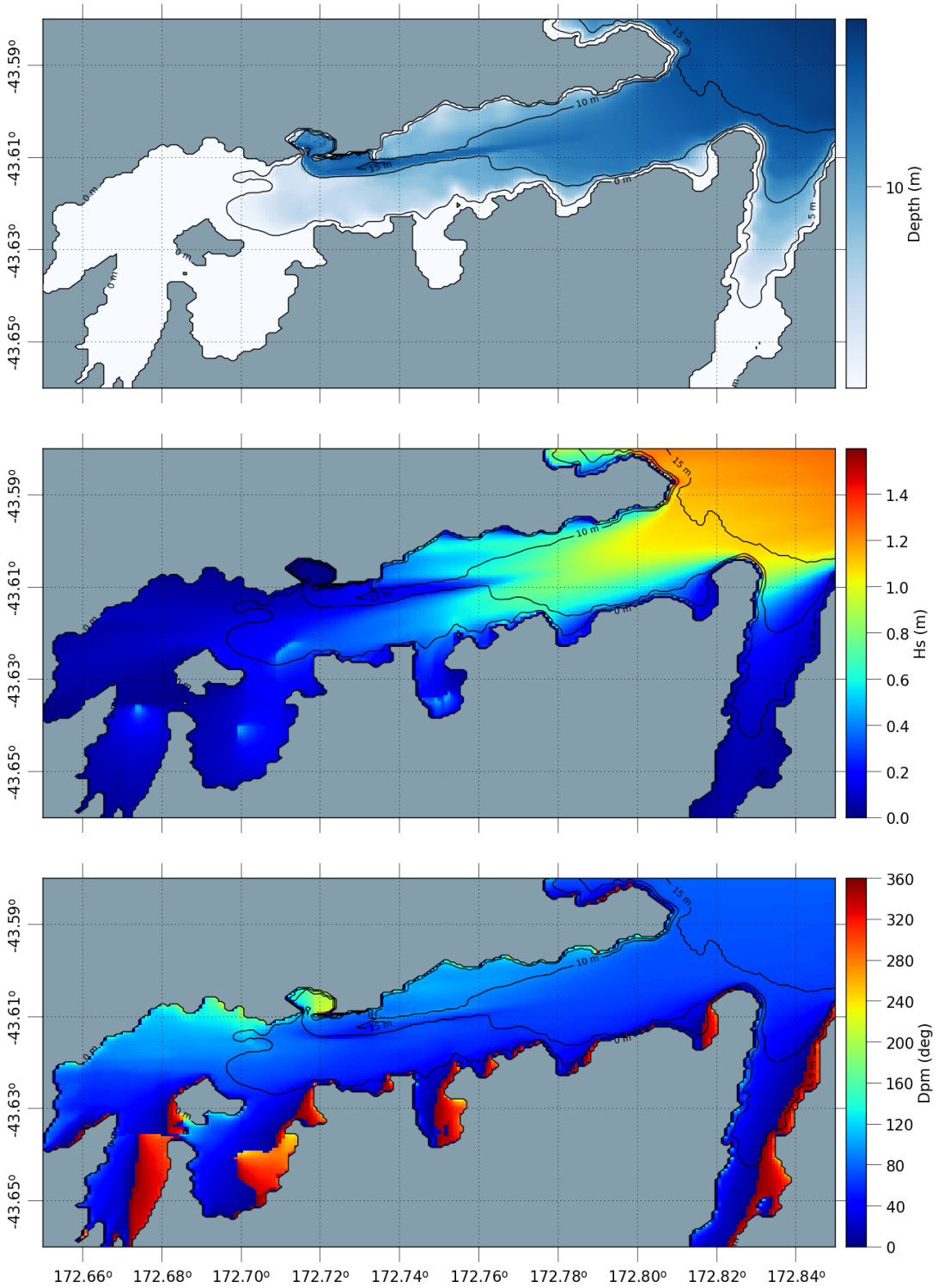


Figure 2.1. Model depths (top) and snapshots of significant wave height (middle) and mean peak wave direction (bottom) for the high-resolution SWAN Lyttelton domain. Model results for the existing channel configuration are shown.

The SWAN model was implemented with wind fields specified from the MetOcean Solutions NZ reanalysis. The dataset was constructed by running the WRF atmospheric model at 12-km resolution, with its initial and lateral boundary conditions set by the Climate Forecast System Reanalysis (Saha et al., 2010) from the National Centers for Environmental Prediction (NCEP). Tidal currents and elevations from a regional tidal model were included in the hindcast wave modelling. The tides were calculated on a 0.06° grid across the entire Banks Peninsula and Lyttelton SWAN domains.

### 2.2.3. Output and post-processing

Gridded wave statistics were calculated over the entire high-resolution Lyttelton SWAN domain. The data were stored in yearly files at three-hour intervals over the 10-year hindcast period. For each modelled frequency-direction wave spectrum $S(f,\theta)$, a one-dimensional frequency spectrum $S(f)$ was calculated as:

$$S_n(f) = \int_{-\pi}^{\pi} E_n(f,\theta) d\theta \tag{2.1}$$

where $E$ is the energy density. The peak frequency $f_p$ was identified as the frequency corresponding to the peak in $S(f)$. The significant wave height $H_s$, mean direction at peak energy $D_{pm}$ and peak wave period $T_p$ were defined as:

$$\begin{aligned} H_s &= 4\sqrt{\int_0^{\infty} S_n(f) df} \\ D_{pm} &= \arctan \frac{\int_{-\pi}^{\pi} E_n(f_p,\theta)\sin(\theta) d\theta}{\int_{-\pi}^{\pi} E_n(f_p,\theta)\cos(\theta) d\theta} \\ T_p &= 1/f_p \end{aligned} \tag{2.2}$$

Wave statistics for the swell and sea wave components were also calculated. The two-dimensional wave spectra were split at 8 sec period with spectral energy above and below 8 sec classified as swell and sea, respectively.

### 2.2.4. Validation

Validation was performed for the Banks Peninsula SWAN domain using significant wave height estimates from satellite altimeter data (Figure 2.2), co-located and compared for the years 2012-2013. Data spikes were removed from the satellite estimates prior to the validation. The following quantitative accuracy measures were calculated from the measured $x_m$ and hindcast, $x_h$ data:

| | | |
|---|---|---|
| Mean absolute error (MAE): | $\overline{\lvert x_h - x_m \rvert}$ | (2.3) |
| RMS error (RMSE): | $\sqrt{\overline{(x_h - x_m)^2}}$ | (2.4) |
| Mean relative absolute error (MRAE): | $\overline{\left\lvert \frac{x_h - x_m}{x_m} \right\rvert}$ | (2.5) |
| Bias: | $\overline{x_h - x_m}$ | (2.6) |
| Scatter Index (SI): | $\frac{\sqrt{\overline{(x_h - x_m)^2}}}{\overline{x_h}}$ | (2.7) |

Good agreement between modelled and satellite estimates of significant wave heights were observed (Figure 2.3). A low-bias of only -0.02 m was observed (Table 2.1), due mostly to a slight under-prediction of very large waves between 4 and 5 m height (see Figure 2.3). Overall the error measures were small (Table 2.1) and the hindcast model replicated the wave height distribution estimate from satellite altimeter data around the Banks Peninsula region.

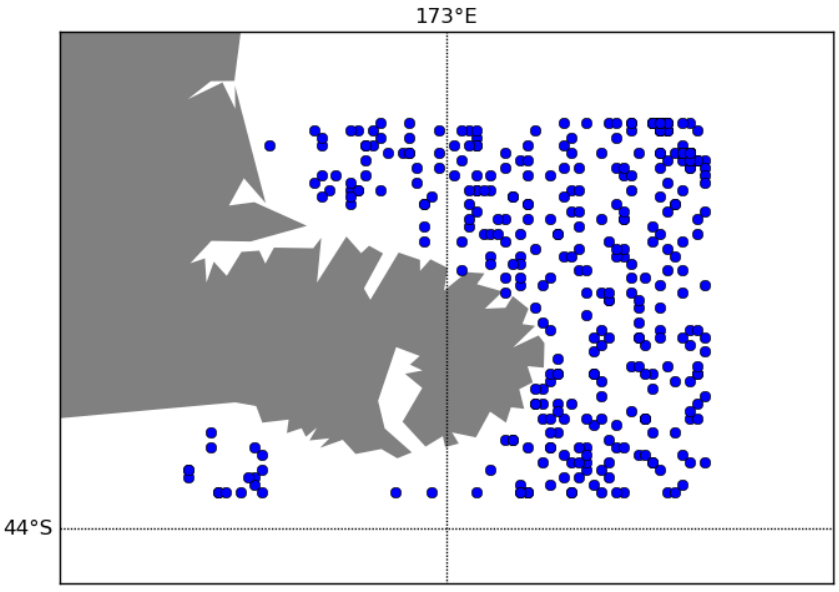


Figure 2.2 Collocated satellite estimates of significant wave height with hindcast values shown as coincident values.

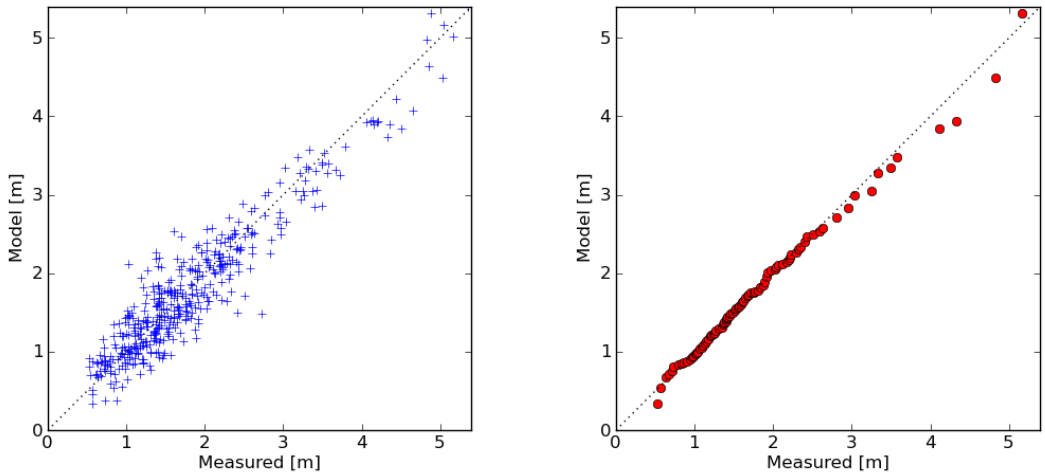


Figure 2.3. Regression plots of sea-swell significant wave height obtained from collocated satellite and raw SWAN hindcast, shown as coincident values (left) and quantile-quantile plot (right).

Table 2.1 Accuracy measures of the hindcast from comparison with satellite estimates of significant wave height.

| | |
|---|---|
| **MAE [m]** | 0.24 |
| **RMSE [m]** | 0.31 |
| **MRAE [%]** | 0.16 |
| **Bias [m]** | -0.02 |
| **SI** | 0.17 |

## 2.3. Hydrodynamic modelling methods

The hydrodynamic model used for the current hindcast was the Regional Ocean Modelling System (ROMS, Haidvogel, et al., 2000). ROMS has curvilinear horizontal coordinate system and solves the hydrostatic, primitive equations subject to a free-surface condition. ROMS is a state-of-the-art model widely used for regional and coastal dynamics assessment. Its terrain-following vertical coordinate system results in accurate modelling of shallow seas with variable bathymetry, allowing the vertical resolution to be inversely proportional to the local depth. Besides tidal and wind-driven currents, ROMS resolves frontal structures and baroclinic pressure gradients. Tidal mixing and turbulent flow are resolved by a separate turbulent closure scheme that is appropriately calibrated for shallow seas.

A three-step nesting approach was employed starting from a New Zealand scale domain (0.08 ˚) and nested domains for the Central East South Island (0.03˚) and Pegasus Bay (0.003˚) to produce a 10-year hydrodynamic hindcast of the hydrodynamics of Pegasus Bay. Details on the model setup and validation are provided in a separate report (MSL P0201-04) and have been published as a conference proceeding paper in Soutelino and Beamsley (2015).

The nesting approach is illustrated in Figure 2.4 and an example of the model output (monthly averaged residual current velocities) is given in Figure 2.5.

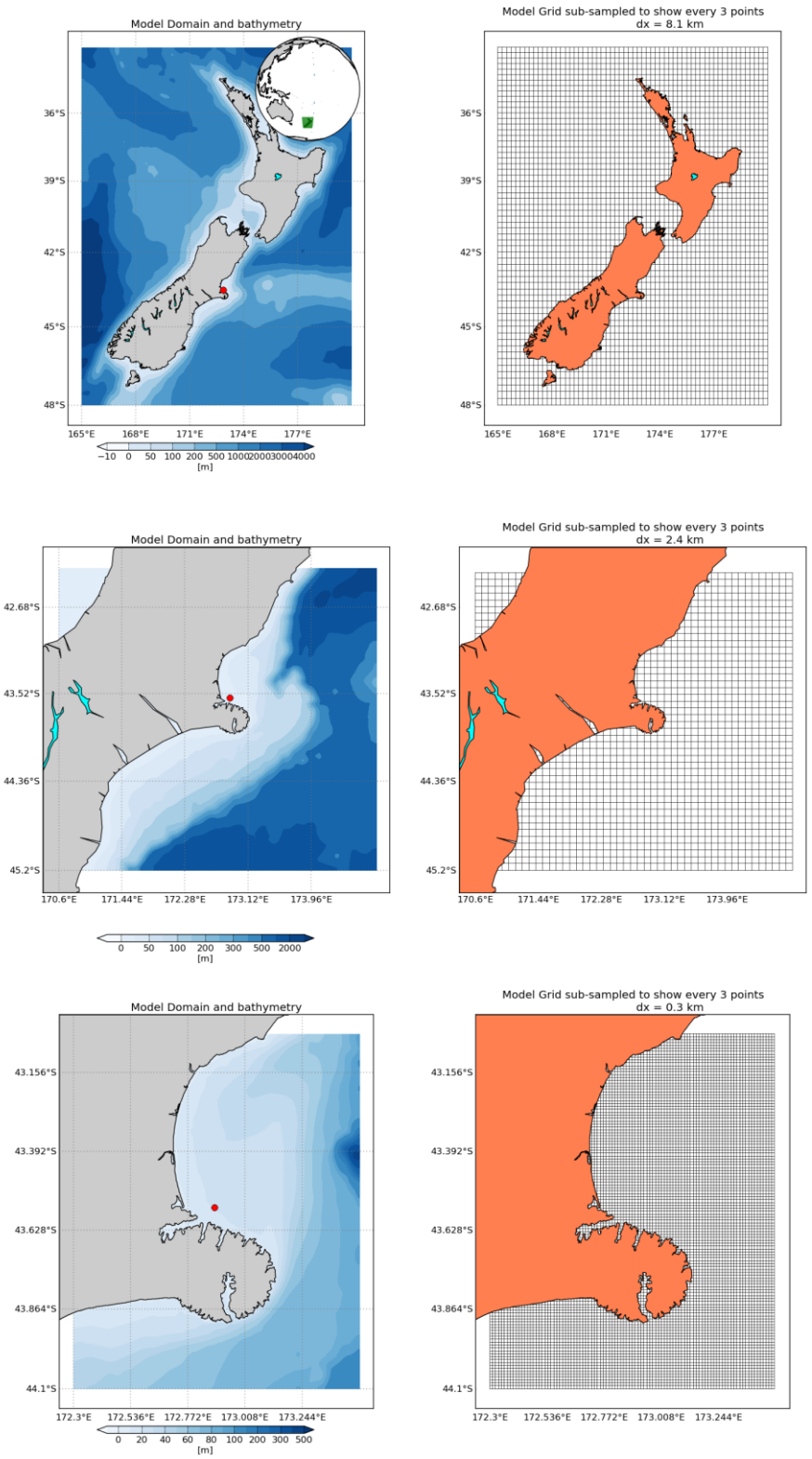


Figure 2.4 Hydrodynamic hindcast downscaling approach with ROMS. Upper panel shows the NZ 0.08 deg domain, middle panel shows the intermediate 0.03 deg Central East South Island (CESI) domain and lower panel shows the 0.003 deg PEGASUS domain. The right panel grids are showing every other 3 grid points, to allow easier graphical interpretation. Land mask is applied to the NW corner of CESI grid.

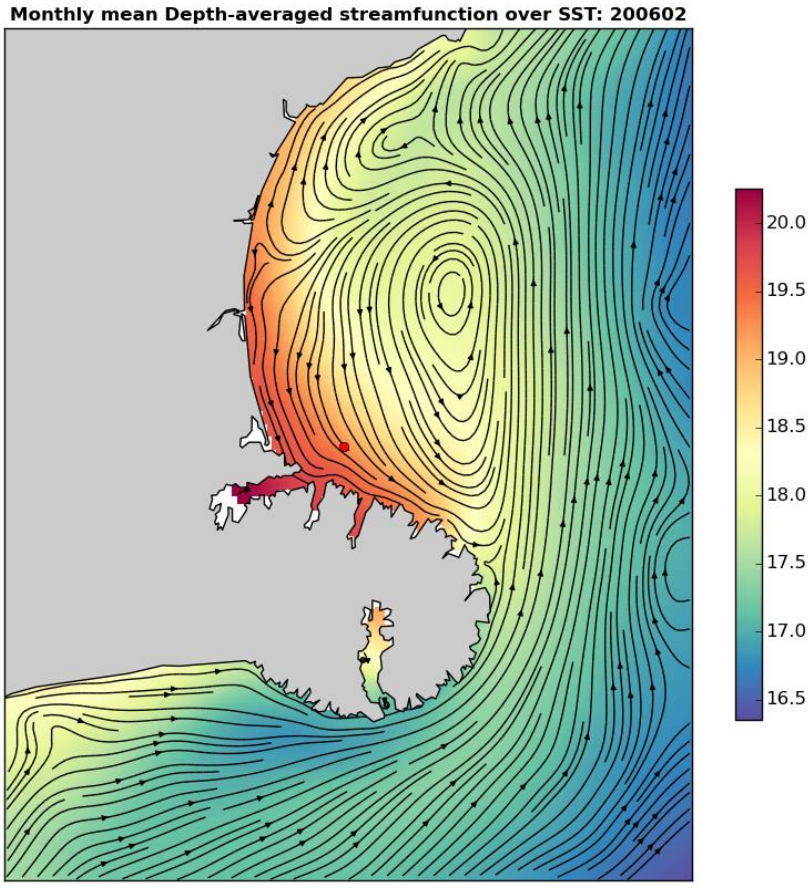


Figure 2.5 Monthly averaged residual flow for February 2006 for the ROMS Pegasus Bay, showing good agreement with literature-based flow features. The dot indicates the position from where current observations were used to validate the model results.

## 2.4. Sediment dynamic modelling methods

The Delft3D numerical model system (e.g. Lesser,. et al., 2004) was used to carry out the numerical simulations of coupled wave, current and sediment transport. The modelling system consists of three modules, with boundary conditions for each supplied from wave and hydrodynamic regional model (SWAN and ROMS respectively):

- Delft3D-WAVE is a nearshore wave propagation model which simulates the evolution of the incoming wave field.
- Delft3D-FLOW is a multi-dimensional (2D or 3D) hydrodynamic model which calculates non-steady flows and transport phenomena that result from tidal, meteorological and wave forcing.
- Delft3D-MOR computes the sediment transport fluxes and the resulting morphodynamic evolution based on the combined action of currents and waves.

The three modules are fully coupled to simulate the morphodynamic feedbacks. Every coupling time step, a new flow field (depth-averaged currents and water levels) is supplied from the hydrodynamic module to the wave module. The wave module propagates waves within the domain, accounting for the ambient hydrodynamics, and in turn provides radiation stress fields and basic wave parameters that are used as forcing by the hydrodynamic module. Delft3D-MOR computes sediment transport based on the combined wave and current action, and updates the seabed morphology; thus affecting subsequent wave and flow computations.

Note that the updating of the seabed morphology can be switched off. In that case, the sediment transport fluxes are computed, but the model bathymetry is left unchanged. This is a useful option for studying general sediment transport pathways, without the unrealistic divergence that can occur due to uncorrected non-linear feedbacks between waves, currents and morphology.

### 2.4.1. Delft3D-WAVE

The third-generation SWAN model (Simulating WAves Nearshore) is used as the wave module (Holthuijsen, 2007). Details of the SWAN model are provided in Section 2.2.1, with boundary conditions supplied from the regional SWAN domains.

For the present work, the local wave model boundary conditions are nested 2D spectral boundaries obtained from a regional scale grid forced either by representative wave events (i.e. accelerated morphological simulations) or real hindcast conditions (i.e. real-time simulations). The nesting allows the retention of spatial variability in the incident wave field due to large scale regional refraction and sheltering effects. Bottom friction was modelled using the formulation of Collins (1972) and the default coefficient value was 0.015. Wave breaking was modelled using a constant critical wave height to water depth ratio of 0.73 with a proportionality coefficient for the rate of dissipation of 1. No meteorological forcing was applied, so friction and wave breaking are the only dissipative mechanisms considered. Due to the scale of the Delff3D model, the exclusion of meteorological forcing is not considered to significantly alter results.

In these simulations, the wave conditions were updated every hour using the hydrodynamic field provided by the hydrodynamic module.

### 2.4.2. Delft3D-FLOW

The hydrodynamic module Delft3D-FLOW solves the Navier-Stokes equations for an uncompressible fluid under the shallow water and Boussinesq assumptions. The system solves the horizontal equations of motion, the continuity equation, the transport equations for conservative constituents, and a turbulence closure scheme. The details of equations and associated sub-models are fully described in Lesser, et al., (2004) and the Delft3D-FLOW user manual (Deltares, 2013b). Water levels, tidal and residual current boundary conditions are supplied from the regional ROMS domain (see Section 2.3).

The model was run in 2D mode, thus providing water levels and depth-averaged flows at each computational time step. The 2D mode is appropriate here as the harbour and surrounding water bodies are expected to be relatively well-mixed (Goring, D., 2009). Bed shear stresses are computed using a standard quadratic friction law. The non-linear enhancement of the bed shear stress in presence of waves was taken into account by means of the wave-current interaction model of Fredsøe, (1984). Turbulence effects are modelled using constant background horizontal and vertical eddy viscosity and eddy diffusivity coefficients. Horizontal background eddy viscosity and diffusivity are set equal to 1 $m^2.s^{-1}$ while a value of $10e^{-6}$ is used for the vertical background viscosity and diffusivity. These values are consistent with recommended values for the resolution of the model grid (Deltares, 2013b).

Water levels were prescribed at the northeast boundary while current boundaries were used for the cross shore and harbour boundaries. The tidal constituents prescribed at the model boundaries were generated from a high resolution tidal model.

A time step of 3 seconds was used for the Delft3D-FLOW simulations, equivalent to maximum Courant numbers of less than 7. The Courant number is a numerical stability criterion that needs to be less than 10 in Delft3D-FLOW (Deltares, 2013b).

### 2.4.3. Delft3D-MOR

The module Delft3D-MOR combines the information provided by the flow and wave modules to compute the sediment transport fluxes at each computational time step. The seabed level can then be updated as a result of the sediment sink and sources terms and computed transport gradients.

The present study considers silt-sized and finer cohesive sediments (< 63 microns) with respect to both the receiving environment (Sneddon, 2009) and the dredge spoil to be disposed (OCEL Consultant Limited, 2013). Geotechnical investigations have indeed identified that the outer harbour seabed sediment can be characterised as a very fine clay/silt mixture typically defined as 1% fine sand (>63 µm), 45% silt (5-50 µm) and 54% clay (<5 µm). Further outside the Harbour heads, the material changes to fine sandy silt but with the silt fraction remaining predominant.

The modelling of transport of cohesive sediment requires an approach that is fundamentally different to mobile sand transport. For very fine sediment size (i.e. silt or clay-sized), the inter-particles forces due to ionic charges

becomes significant relative to the gravitational forces which strongly dominate the sand transport processes. As a result, processes including flocculation, hindered settling, and bed consolidation have important roles in the movement of cohesive particles. Description of the associated sub-models is included the Delft3D FLOW manual (Deltares, 2013b).

The cohesive sediment transport is calculated by solving the advection-diffusion equation for the suspended sediment. Note that no bed load transport is considered for the cohesive sediment in Delft3D (see Deltares, 2013b),

$$\frac{\partial C}{\partial t}+\frac{\partial uC}{\partial x}+\frac{\partial vC}{\partial y}+\frac{\partial (w-w_s)C}{\partial z}= \frac{\partial}{\partial x}\left(\varepsilon_{s,x}\frac{\partial C}{\partial x}\right)+\frac{\partial}{\partial y}\left(\varepsilon_{s,y}\frac{\partial C}{\partial y}\right)+\frac{\partial}{\partial z}\left(\varepsilon_{s,z}\frac{\partial C}{\partial z}\right) \quad (2.8)$$

where,

| | |
|---|---|
| $E$ | Mass concentration [kg.m$^{-3}$] |
| $u, v, w$ | Velocity components [m.s$^{-1}$], |
| $\varepsilon_{s-x,y,z}$ | Eddy diffusivities in the x,y,z directions [m$^2$.s$^{-1}$], |
| $w_s$ | Sediment settling velocity [m. s$^{-1}$]. |

Sediment fluxes between the water phase and the bed are calculated using the Partheniades-Krone formulations (Partheniades,1965).

$$E = M.S(\tau_{cw}, \tau_{cr,erosion}) \quad (2.9)$$

$$D = w_s.c_b.S(\tau_{cw}, \tau_{cr,deposition}) \quad (2.10)$$

$$c_b = c(z = \frac{\Delta z_b}{2}, 2) \quad (2.11)$$

where,

| | |
|---|---|
| $E$ | Erosion flux [kg/m$^{-2}$.s$^{-1}$] |
| $M$ | User-defined erosion parameter [kg.m$^{-2}$.s$^{-1}$] |
| $S(\tau_{cw}, \tau_{cr,erosion})$ | Erosion step function: |

$$S(\tau_{cw}, \tau_{cr,erosion}) = \begin{cases} \left(\frac{\tau_{cw}}{\tau_{cr,erosion}} - 1\right), & when\ \tau_{cw} > \tau_{cr,erosion} \\ 0 & ,when\ \tau_{cw} > \tau_{cr,erosion} \end{cases} \quad (2.12)$$

| | |
|---|---|
| $D$ | Deposition flux [kg.m$^{-2}$.s$^{-1}$] |
| $M$ | User-defined erosion parameter [kg.m$^{-2}$.s$^{-1}$] |
| $w_s$ | Sediment settling velocity [m. s$^{-1}$]. |
| $c_b$ | Average sediment concentration near bottom [kg.m$^{-3}$] |

$$S(\tau_{cw}, \tau_{cr,deposition}) = \begin{cases} \left(\frac{\tau_{cw}}{\tau_{cr,deposition}} - 1\right), & when\ \tau_{cw} > \tau_{cr,erosion} \\ 0 & ,when\ \tau_{cw} > \tau_{cr,erosion} \end{cases} \quad (2.13)$$

| | |
|---|---|
| $\tau_{cw}$ | Maximum bed shear stress due to current and waves. |
| $\tau_{cr,erosion}$ | User defined critical erosion shear stress [N. m$^{-2}$] |
| $\tau_{cr,deposition}$ | User defined critical deposition shear stress [N. m$^{-2}$] |

Erosion and deposition terms are finally used as bed boundary conditions;

$$-w_s.C - \varepsilon_{s,z}\frac{\partial C}{\partial z} = D - E\ ,\ at\ z = z_b \quad (2.14)$$

The formulation requires the specification of erosion and deposition shear stresses. The critical erosion shear stress is now a widely accepted concept that is the shear stress magnitude that must be exceeded before sediment motion is initiated. In contrast, the existence of a critical deposition shear stress, which is a threshold shear stress over which no deposition can occur, is still debated. In the present study the critical deposition shears stress was set to a very large value of 1000 N.m$^{-2}$, which is never exceeded, so that deposition can occur continuously and without any restrictions related to the ambient shear stress.

### 2.4.4. Model domains

The Delft3D FLOW model uses a curvilinear grid that includes the shoreline from New Brighton to Pigeon Bay (~20 km) and extends 13 km offshore to depth of about 22 metres relative to CD (Figure 2.6). Grid resolution ranges from 30 m to ~ 400 m with increased resolution focused over the disposal ground, channel and shallow nearshore areas. The grid used for the local wave model has half of the flow grid resolution with grids point positions identical to flow grid points. Three additional grid lines are located on the eastern, western and northern side relative to the flow grid to avoid flow disturbance near the model boundaries. A larger scale grid including the wider Pegasus Bay was used to simulate the transformation of the offshore wave climate to the nested high-resolution wave model boundaries (Figure 2.7).

To simulate the sediment dispersion following the disposal of the dredged sediment from the channel, a post-disposal bathymetry was estimated by deepening the channel to the projected depth and considering the totality volume expected to be disposed (18 million m$^3$) distributed over the proposed ground extents (~12.5 km$^2$), equivalent to a homogeneous depth increase of 1.44 m over the ground. Note that this is a conservative approach, since in reality the sediment volumes will be disposed and naturally dispersed progressively over the potentially two separate dredging work periods, each taking between 9-14 months. Additionally, a fraction of the total volume will also be dispersed immediately following release, before settling within the disposal ground.

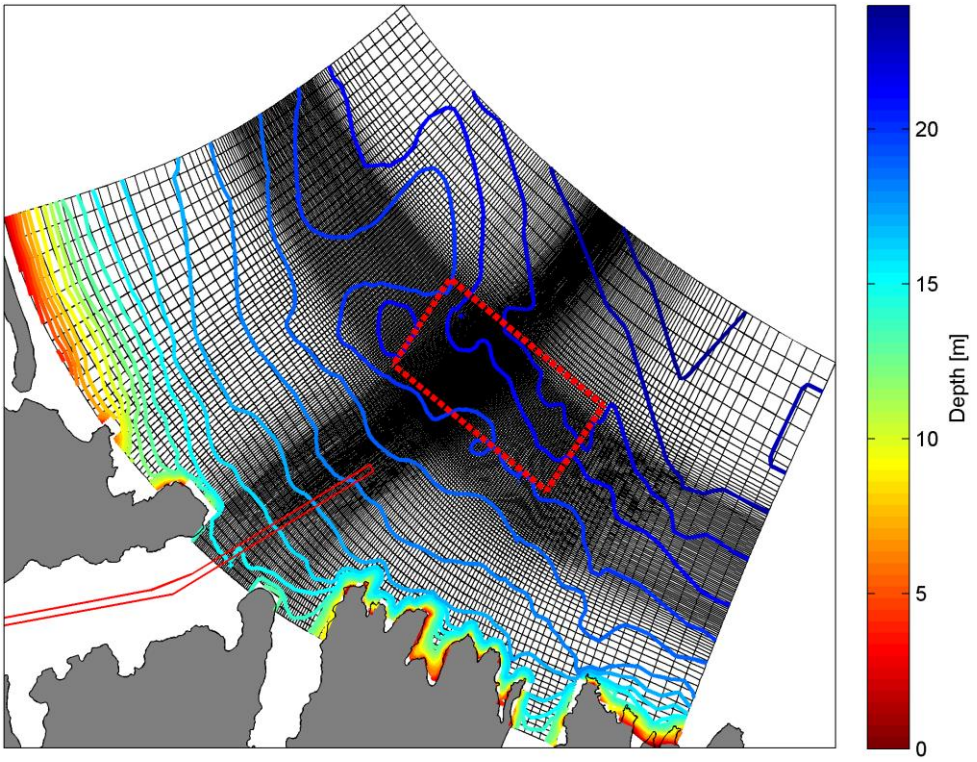


Figure 2.6 Delft3D – FLOW model grids. The disposal ground and new channel are shown in red.

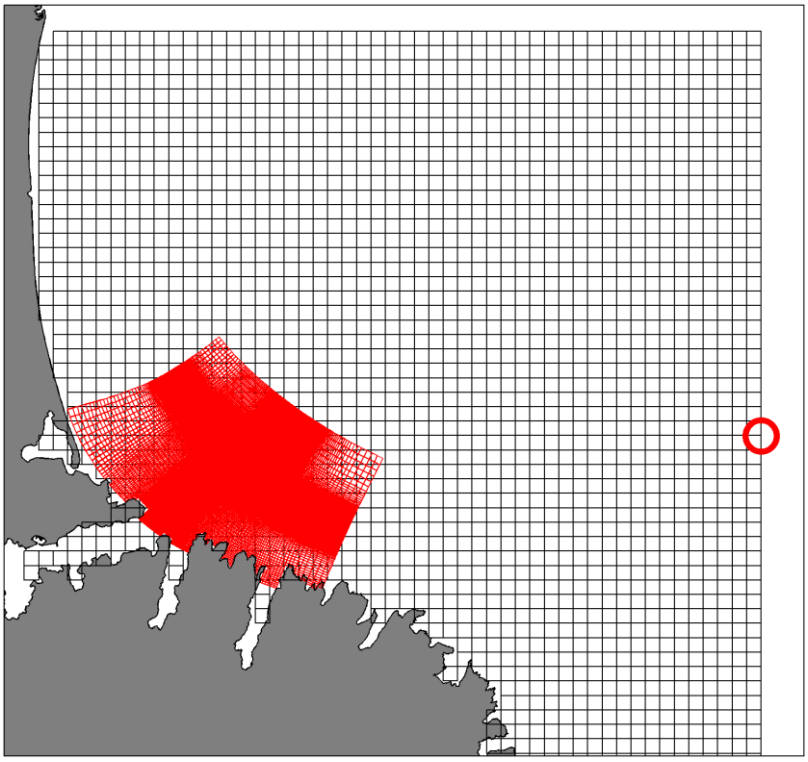

Figure 2.7 Delft3D – WAVE regional and local model grids. The red dot indicates the location used for the wave climate reduction.

### 2.4.1. Model Setup

In the present application, the sediment transport model is driven by wave and flow fields that are nested within calibrated high resolution regional waves and hydrodynamics models. The calibration of sediment transport models is a more complicated process because it requires extensive field data on the underlying sediment composition and estimates of the rheology of the disposed sediment. Typically this calibration is done using historical morphological behaviour – such as a previous dumping exercise. As this is a new disposal ground, and large scale morphological studies have not been undertaken in these environs, such information was not available here.

As outlined in section 2.4.3, the sediment transport requires the input of a range of numerical and physical parameters that eventually control the sediment movement. In the present study, the available empirical information on the sediment to be disposed provided some guidance on appropriate ranges for the parameters characterising the sediment type, such as the settling velocity, or critical shear stress. The choice of other parameters, notably the erosion factor, is more arbitrary in absence of detailed local information. Some sensitivity analysis was performed to identify the effects of these key parameters within recommended default ranges and indicated that model predictions varied depending of the parameters combination. Accordingly, the sediment transport and morphological models remain uncalibrated and quantitative predictions should be interpreted carefully. However, the predicted patterns of morphological changes are expected to remain valid, and the qualitative predictions can provide useful insight on the governing processes.

As outlined in the previous section, sediment sampling indicated that the sediment within the Harbour that is expected to be dredged consists of fine clay/silt mixture typically defined as 45% silt (5-63 μm) and 54% clay (<5 μm) and only 1% of fine sand (>63 μm). It is expected that the sediment texture changes to a fine sandy silt outside of the Harbour and further offshore within Pegasus Bay although less empirical data is available. To investigate the fate of the sediment disposed within the proposed disposal ground, the total volume of (cohesive) sediment to be dredged was spread homogenously throughout the disposal ground resulting in a sediment thickness of 1.44 m. This is a conservative assumption given the ground loading will be spread over time which tends to result in large dispersal rates from the ground in the models, however, it is useful to provide a picture of dispersal patterns from all regions of the ground.

Rather than make assumptions of the composition of the underlying seabed, for which less empirical information is available, sediment thickness was set to zero elsewhere. The approach focuses on the net effect of the additional sediment volume artificiality input to the Pegasus Bay system through the disposal activities and assumes the remainder of the seabed in the vicinity of the disposal ground is in a state of equilibrium.

The typical range of critical shear stress of weakly consolidated mud beds is ~0.1-0.3 $N.m^{-2}$ (e.g. Van Rijn, 2007a). Here, a generic value of 0.2 $N.m^{-2}$ was used. With respect to the sediment settling velocity, the cohesive nature of the clay/silt material typically result in the formation of aggregates or “flocs”, which settle much faster than the individual particles making up the flocks. (e.g. Van Rijn, 2007b). In the absence of in-situ measurements on the settling of such flocculated cohesive sediment at the site, a generic settling velocity of 1 $mm.s^{-1}$ was used, based on available guidance for such

aggregates (e.g. Whitehouse et al., 2000, Spearman pers. comms., 2015). The value of erosion parameter used for the presented simulations was 1e-5. The model parameters used for the study are summarized in Table 2.2.

Table 2.2 Delft3D model parameters.

| Parameter | Description | Value |
|---|---|---|
| ***Wave*** | | |
| BedFriction | Seabed friction formulation | Collins |
| | | Collins (1972) |
| BedFricCoef | Collins's frictions coefficient | 0.015 |
| Breaking | Depth induced breaking model | TRUE |
| | | ( Battjes and Janssen,1978) |
| BreakAlpha | Rate of dissipation | 1 |
| BreakGamma | Breaker parameter Hmax/h | 0.73 |
| WaveSetup | Wave-induced setup model | TRUE |
| ***Hydrodynamics*** | | |
| Dt | Computational time step | 3 s. |
| DryFlc | Minimum depth for drying/flooding | 0.1 |
| Vicouv | Horizontal background eddy viscosity | 1 |
| Dicouv | Horizontal background eddy diffusivity | 10 |
| Vicoww | Vertical background eddy viscosity | 1.00E-06 |
| Dicoww | Vertical background eddy diffusivity | 1.00E-06 |
| Rouwav | Model for bottom stress formulation due | #FR84# |
| | to combined wave and current action | (Fredsoe, 1984) |
| Roumet | Chézy Coefficient | #C# |
| Ccofu,Ccofv | | 70 |
| ***Sediment transport*** | | |
| *Cohesive Sediment* | | |
| RhoSol | Sediment density [kg/m3] | 2650 |
| WSM | Sediment settling velocity [m/s] | 1.00E-03 |
| CDryB | Dry bed density [kg/m3] | 500 |
| IniSedThick | Initial sediment layer thickness [m] | 1.44 in the ground (0 elsewhere) |
| TcrSed | Critical deposition shear stress [n/m2] | 1000 |
| TcrEro | Critical erosion shear stress [n/m2] | 0.2 |
| EroPar | Erosion Parameter | 1.00E-05 |

### 2.4.1. Sensitivity testing the erosion parameter

In the absence of calibrating the morphological modelling, results need to be considered as qualitative not quantitative. As such, the general patterns or erosion and accretion predicted by the model are expected to be consistent irrespective of the parameters used within the model.

The key parameter in predicting the entrainment and transport of the surficial sediment within the modelling parameters is the user defined Erosion Parameter (*M*) which has units of $kg.m^{-2}.s^{-1}$. For soft cohesively bound beds Winterwerp, et al., (2012) found computed and measured values of the erosion parameter to range between approximately $1x10^{-3}$ and $1x10^{-7}$.

Sensitivity testing of the Lyttelton Harbour environs has been undertaken by modelling the entire existing environment (see Figure 2.8) in the absence of either the proposed dredge channel or sediment available at either the maintenance or proposed capital disposal grounds. The domains were seeded assuming a constant depth of available sediment of 0.25 m. An Erosion Parameter (M) of $1 \times 10^{-5}$ and $1 \times 10^{-5}$ were tested.

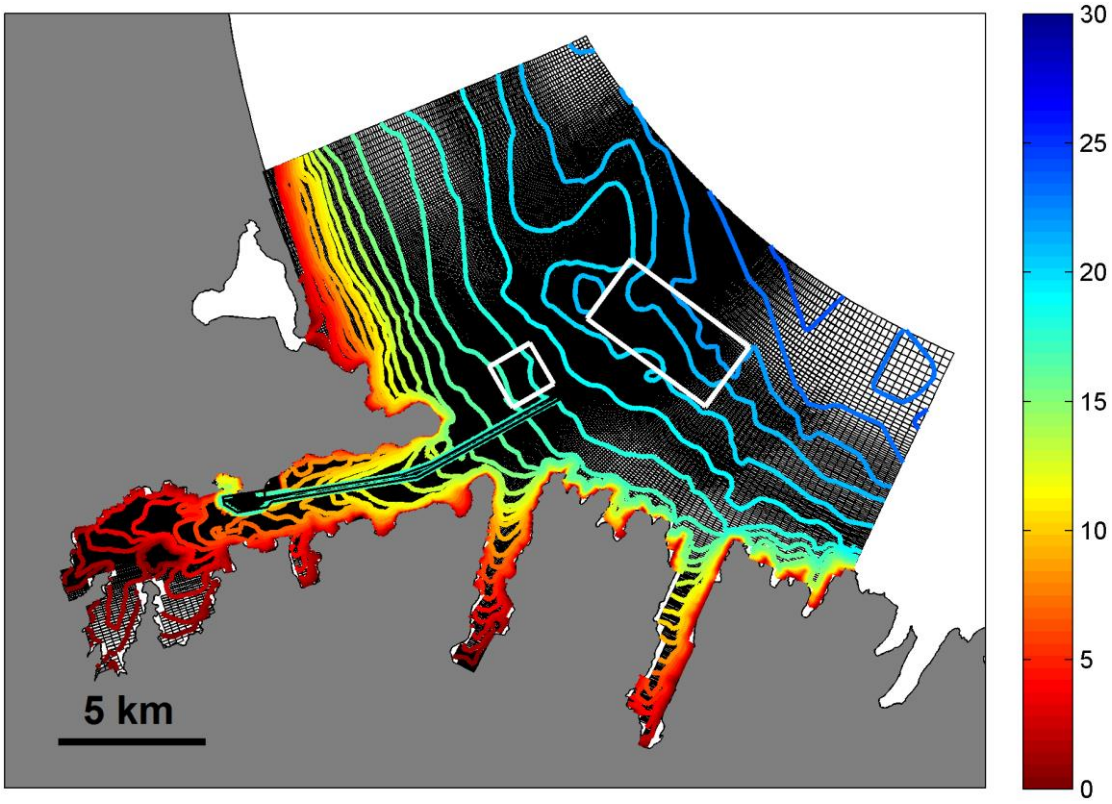


Figure 2.8 New model grid including the entire Lyttelton Harbour/Whakaraupō and coastlines from Brighton/Sumner to Pigeon Bay.

# 3. SENSITIIVITY TESTING

The effect of changing the user defined Erosion Parameter on the predicted bed level changes for the existing environment (without capital dredged channel or capital and maintenance disposal grounds) is shown in Figure 3.1. Effectively, the erosion parameter scales the predicted bed level changes approximately linearly; with higher rates (i.e. $1 \times 10^{-5}$) resulting in increased bed level changes, while the general pattern is persistent.

Irrespective of port operations, the model predicts sedimentation within the entrance to Port Levy/Koukourārata, while erosion is predicted within the entrance to Port Lyttelton/Whakaraupō. While the general patterns of erosion / accretion are likely to be accurate, without calibration or validation of the model using measured data these results can only be assessed based on anecdotally evidence, which suggests that an Erosion Parameter of $1 \times 10^{-6}$ more accurately represents what is seen within the environs, particularly within the entrance to Port Levy/Koukourārata.

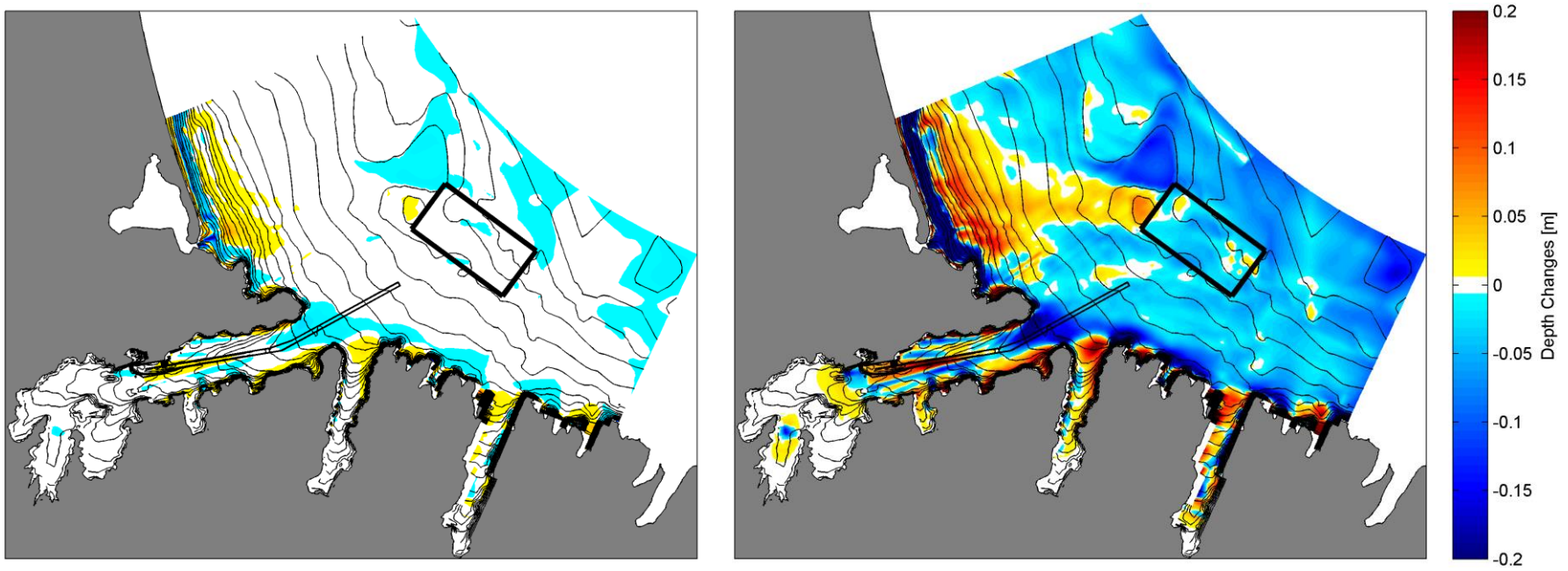


Figure 3.1 Sensitivity testing of the user defined Erosion Parameter (M) assuming a constant depth of available sediment (0.25 m) within the entire domain and assuming existing conditions, i.e. excluding the proposed dredged channel or sediment on either the proposed offshore capital or maintenance grounds. Erosion parameter of $1x10^{-6}$ is shown on the left, while Erosion Parameter of $1x10^{-5}$ is shown on the right.

# 4. MORPHOLOGY MODELLING TECHNIQUES

This section details the two morphology modelling approaches employed in this study.

- Medium-term morphological modelling, and
- Real time simulations

Medium-term morphological modelling aims to reproduce the morphological evolution on time scale from months to years using a reduction of inputs combined with acceleration techniques to ensure reasonable computational times.

Real time simulations reproduce the exact chronology of wave and tidal forcing within a historical context to predict instantaneous sediment transport fields and the associated bathymetric adjustments.

Both techniques used in the morphology modelling consider waves and tidal flows, as well as the influence of meso-scale, regional currents.

## 4.1. Medium-term morphological modelling

The main challenge with applying process-based models to predict morphological evolution is that the morphological behaviour of coastal systems generally develops over time scales several orders of magnitude larger than the time scale of the hydrodynamic fluctuations driving the sediment transport (i.e. hours to days versus years to decades and more). This means that a model system that is able to predict the time series of instantaneous hydrodynamics and sediment transport will require an unfeasibly long period of time to compute a multi-year real time simulation. Instead, several strategies are commonly used to simplify and accelerate the modelling of medium to long term morphological evolution (i.e. De Vriend, et al., 1993; Roelvink J.A., 2006). The approach employed here combines the reduction of the input forcing (i.e. wave, tides, current residuals) with the use of morphological factors, which is one of the most commonly applied method (e.g. Dastgheib, A., 2012; Lesser, 2009; Lesser, et al., 2004).

Input reduction essentially means selecting a limited number of representative forcing conditions (i.e. current velocities and wave) that will reproduce the medium-term residual sediment transport patterns and associated morphological evolution (De Vriend, et al., 1993). The morphological factor is a technique to improve computational efficiency by accelerating computed morphological evolution. The application of these techniques to the present study is explained in the following sections.

### 4.1.1. Tidal input reduction

Astronomical tides are deterministic and can therefore be accurately predicted for any period of time. However tidal oscillations exhibit significant long-term modulations (e.g. spring/neap, yearly and nodal cycles), which make chronological simulations of such cycles computationally demanding.

The basis for tidal input reduction is to find a *representative* tide that most closely reproduce the net and gross sediment transport as the naturally

varying tides over the region of interest and for the time period considered. In the present study, the *representative* tide was determined following the approach of Latteux, (1995), which is commonly applied (e.g. Brown and Davies, 2009; Dastgheib, 2012; Grunnet, et al., 2004). Given the duration of the simulations that are to be undertaken in this study (i.e. 1 year), the salient mover required to be accurately captured is the residual effects of the spring-neap oscillations; so a time period of 12 cycles was considered necessary.

Tidal signals at a reference point located at the centre of the initially proposed disposal ground (see Figure 4.1) were generated from a high resolution tidal constituent grid, and time series of sediment transport were estimated using a simple power law $Q=A.u^{b}$ ($Q$ is the transport flux, $A$ is a constant factor, $u$ is current velocity, $b$=5 following Engelund and Hansen, (1967). The single tide that best reproduces the net and gross transport magnitude was identified and used in the accelerated simulations. The representative tide is compared to *M2* tidal signals in Figure 4.2.

The representative tide has a period of 12.5 hours which is very close to the *M2* component period and an elevation range of 1.95 m, which is ~14% larger than the mean range. The representative tide range is generally expected to be larger than the mean range due to strong non-linear relationship between flow velocity and sediment transport. Latteux's. (1995) findings suggest that a representative tide range is usually 7 to 20% larger than mean range (mainly depending on the transport formulation used) which is consistent with ratio obtained here. Similar ratios have also been used in Grunnet, et al., (2004), and Lesser, (2009).

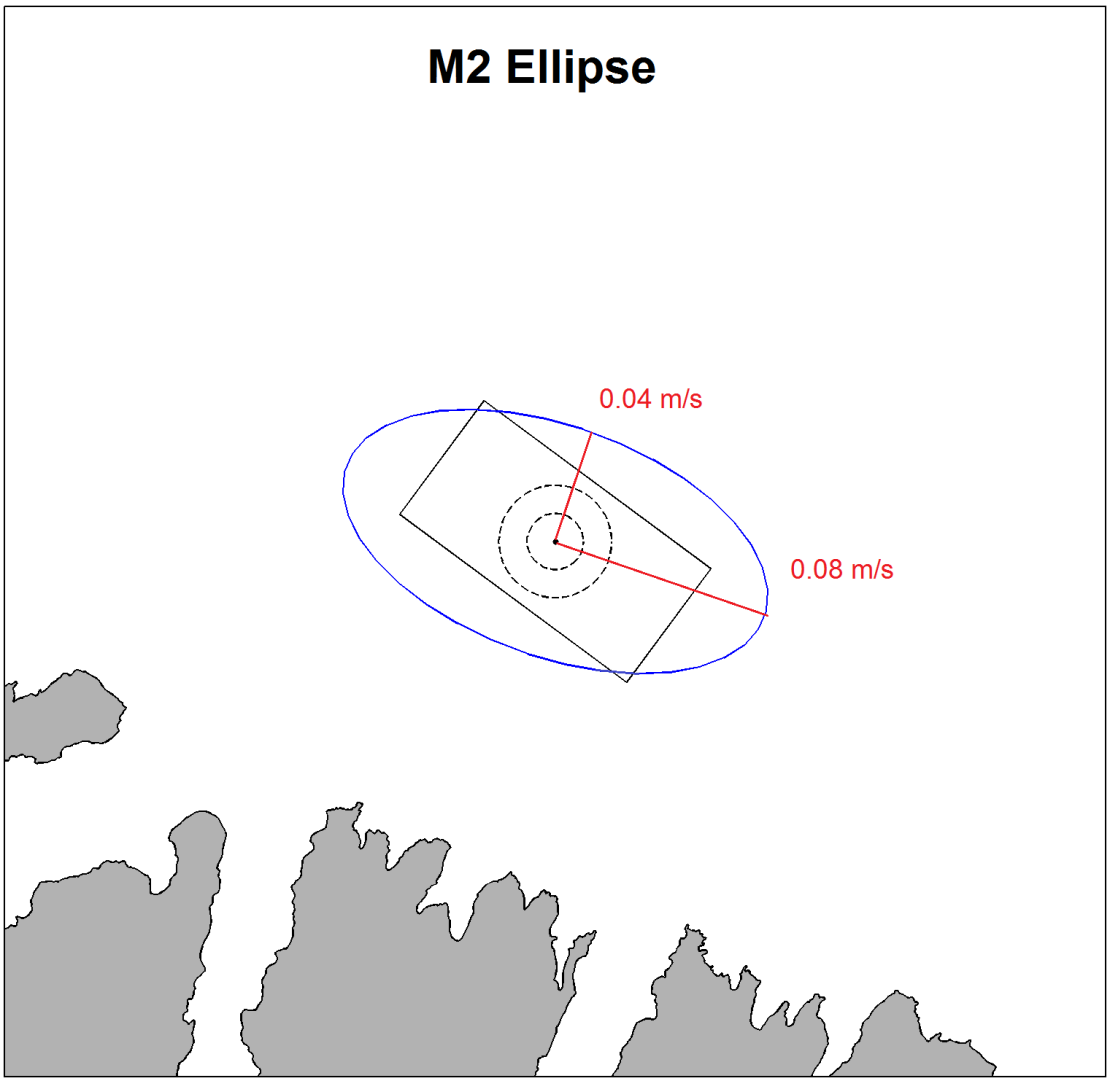


Figure 4.1 Reference site used for the definition of the representative tide with M2 tidal ellipse. The proposed disposal ground is shown in black.

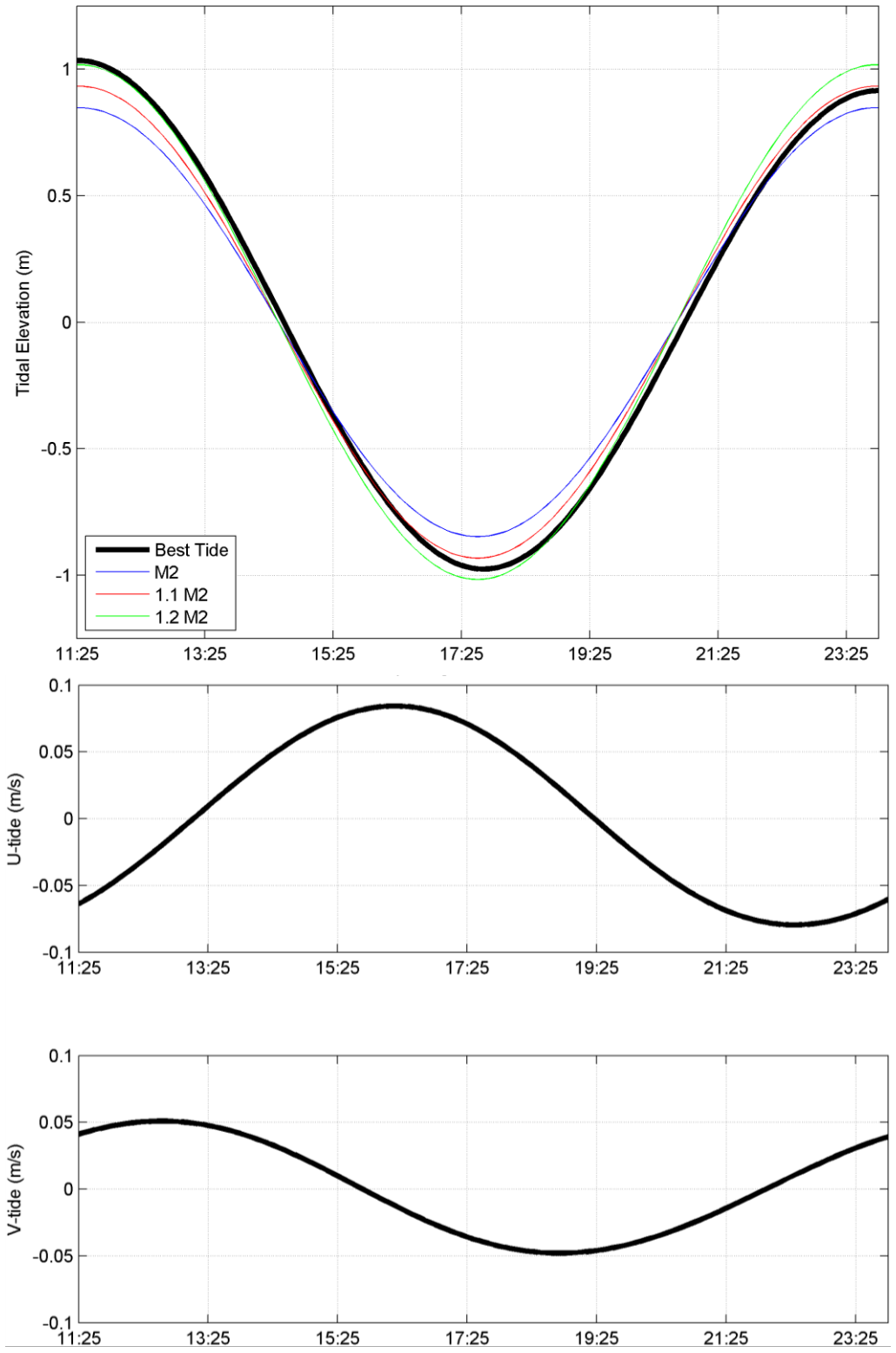


Figure 4.2 Tidal elevation and currents at the centre of the proposed disposal ground (see Figure 4.1) during the representative tide. The coloured lines on the top plots shows pure M2 tide elevation curves with amplitudes timed by 1, 1.1, and 1.2 for comparison.

### 4.1.2. Wave input reduction

The objective of wave input reduction is to define a set of offshore wave boundary conditions which reproduce the same residual sediment transport patterns and morphological evolution as the real time forcing over a given time period. The approach employed here follows the input reduction framework provided in Lesser, (2009) and Walstra et al., (2013).

The first step is the selection of a reduction period, which is the length of the real-time wave time series that is used to define the representative conditions. This is typically governed by the time scale of the morphological evolution of interest (e.g. monthly, seasonal, annual behaviour). In the present study, the reduction was undertaken based on a 10 year hindcast wave climate obtained from SWAN simulations, used to define an average annual wave climate. A wave condition time-series was extracted at the middle of the eastern boundary of the wave model domain (Figure 2.7). In a second step, a set of representative wave classes are defined by distributing the discrete wave data points into a finite number of height and direction bins, and computing a ***representative*** value for each bin.

The basic method to determine a ***representative*** value within a bin is to use a weighted average of the data points by their frequency of occurrence:

$$F_{rep,j} = \frac{\sum_{i=1}^{n} f_i . F}{\sum_{i=1}^{n} f_i} \tag{3.1}$$

where *F* represents the wave height, period or direction, *f* is the frequency of occurrence of the wave condition *i* and n is the number of data points within a bin.

To account for the non-linear dependence of sediment transport on wave height, an additional weighting can be applied for the computation of the representative height:

$$H_{s,rep,j} = \left( \frac{\sum_{i=1}^{n} f_i . H_{s,i}^{p}}{\sum_{i=1}^{n} f_i} \right)^{1/p} \tag{3.2}$$

where *p* is the power to which the sediment transport is assumed to be related to the wave height. Typically *p* is set to between 2 to 3. The exponent ensures that larger waves will have a relatively greater contribution in the computation of the representative wave height.

Here Eq. 3.2 was used with a value of $p$ = 2.5 which corresponds with the CERC formula for longshore transport (Coastal Engineering Research Center, 1984) and is frequently used to estimate the morphological impact of waves. Associated representative periods and directions were determined using the same weighting as the wave height.

The initial wave data binning is relatively arbitrary and can be equidistant or non-equidistant (i.e. varying bin size). In the non-equidistant case, bins can be defined following either (subjective) scientific judgment or more objective approaches. Here, the height and direction bins were defined so that the relative “morphological impact of waves” was similar in each bin (Dastgheib, A., 2012; Lesser, 2009).

The morphological impact of waves of a given wave class was estimated according to:

$$M_j = p_j \,.\, H_{s,rep,j}^{2.5} \tag{3.3}$$

where $p_j$ is the probability of occurrence of the bin $j$, and $H_{s,rep,j}$ the representative wave height of that bin (Lesser, 2009). Note that this is equivalent to "potential sediment transport" indicator used in Dastgheib, (2012).

To automate the determination of bin limits, this indicator was initially computed for a joint probability of wave height and direction with very fine equidistant bins ($\Delta H$=0.1 m, $\Delta Dir$=2 deg.). Based on the number of directional and wave height bins to be used for the classification, the directional bin limits are determined first, in a way that the sum of the morphological impact of waves $M_j$ within each bin is (approximately) equal. The same principle is then used within each of these directional bins to define the wave height bin limits. This way, the "morphological impact of waves" is similar in each bin.

The offshore wave climate in Pegasus Bay consists of predominant southerly swell conditions mixed with less frequent wave events from the southeast and northeast quarters (Figure 4.3). The most northerly events are generally locally generated with lower wave periods, but can still be relatively energetic in terms of wave heights (i.e. up to 3.5 m and more). At the disposal site, this results in wave conditions from the east-northeast quadrant (Figure 4.4) due to refraction effects around Banks Peninsula, with a mean wave height of 0.9 m (Table 4.1).

The wave climate classification used in the following morphological simulations was defined using 3 directional bins and 3 wave height bins. The general classification obtained for the average annual wave climate at the reference site reproduces the three main groups of wave events from the south, southeast and northeast direction (Figure 4.5) experienced at the site. The wave height delimitations are relatively consistent with a first class, with wave heights below 2 m being the most frequent, a second with wave heights from 2 to 3 m and the highest energy group having wave heights larger than ~3 m.

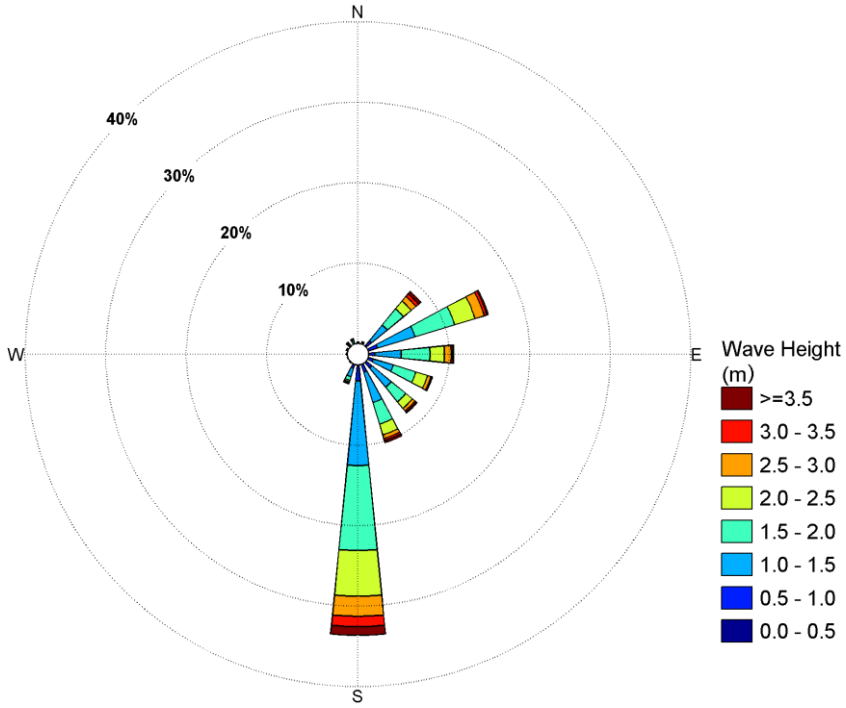


Figure 4.3 Wave rose from the 10 year wave climate at a site located at the centre of the regional wave domain eastern boundary (see Figure 2.7).

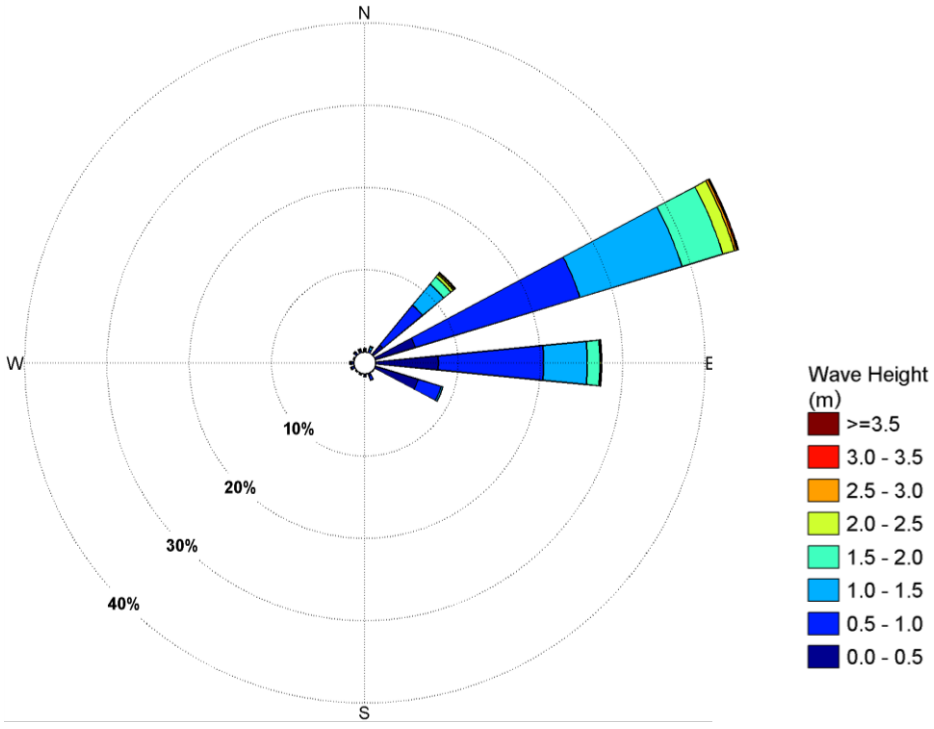


Figure 4.4 Wave rose from the 10 year wave climate at the centre of the proposed disposal ground (see Figure 4.1).

Table 4.1 Wave heights statistics at the centre of the proposed disposal ground.

| | min | mean | median | p90 | p95 | p99 | max |
|---|---|---|---|---|---|---|---|
| **January** | 0.01 | 0.92 | 0.84 | 1.54 | 1.73 | 2.25 | 3.33 |
| **February** | 0.18 | 0.91 | 0.78 | 1.53 | 1.75 | 2.55 | 3.73 |
| **March** | 0.20 | 0.85 | 0.75 | 1.38 | 1.66 | 2.29 | 3.14 |
| **April** | 0.19 | 0.86 | 0.77 | 1.54 | 1.83 | 2.24 | 3.42 |
| **May** | 0.12 | 1.00 | 0.93 | 1.65 | 1.92 | 2.62 | 4.59 |
| **June** | 0.18 | 0.95 | 0.85 | 1.72 | 2.04 | 2.91 | 4.41 |
| **July** | 0.16 | 0.96 | 0.84 | 1.72 | 2.01 | 2.96 | 3.78 |
| **August** | 0.13 | 1.04 | 0.93 | 1.80 | 2.00 | 2.65 | 3.32 |
| **September** | 0.17 | 0.87 | 0.78 | 1.43 | 1.69 | 2.18 | 3.42 |
| **October** | 0.13 | 0.78 | 0.69 | 1.29 | 1.51 | 2.21 | 4.00 |
| **November** | 0.12 | 0.80 | 0.72 | 1.32 | 1.53 | 2.13 | 3.39 |
| **December** | 0.11 | 0.87 | 0.78 | 1.42 | 1.64 | 2.46 | 3.32 |
| **2004** | 0.17 | 0.89 | 0.78 | 1.50 | 1.83 | 2.76 | 4.41 |
| **2005** | 0.11 | 0.83 | 0.72 | 1.42 | 1.75 | 2.41 | 3.57 |
| **2006** | 0.12 | 0.85 | 0.76 | 1.46 | 1.75 | 2.16 | 2.71 |
| **2007** | 0.12 | 0.80 | 0.69 | 1.36 | 1.61 | 2.09 | 3.65 |
| **2008** | 0.13 | 0.97 | 0.89 | 1.64 | 1.88 | 2.74 | 3.78 |
| **2009** | 0.15 | 0.90 | 0.76 | 1.55 | 1.80 | 2.61 | 3.28 |
| **2010** | 0.16 | 0.96 | 0.86 | 1.64 | 1.91 | 2.62 | 4.59 |
| **2011** | 0.13 | 0.94 | 0.83 | 1.61 | 1.91 | 2.53 | 3.97 |
| **2012** | 0.01 | 0.93 | 0.84 | 1.56 | 1.81 | 2.28 | 3.54 |
| **2013** | 0.18 | 0.96 | 0.87 | 1.59 | 1.82 | 2.25 | 3.06 |
| **All** | 0.01 | 0.90 | 0.80 | 1.54 | 1.82 | 2.44 | 4.59 |

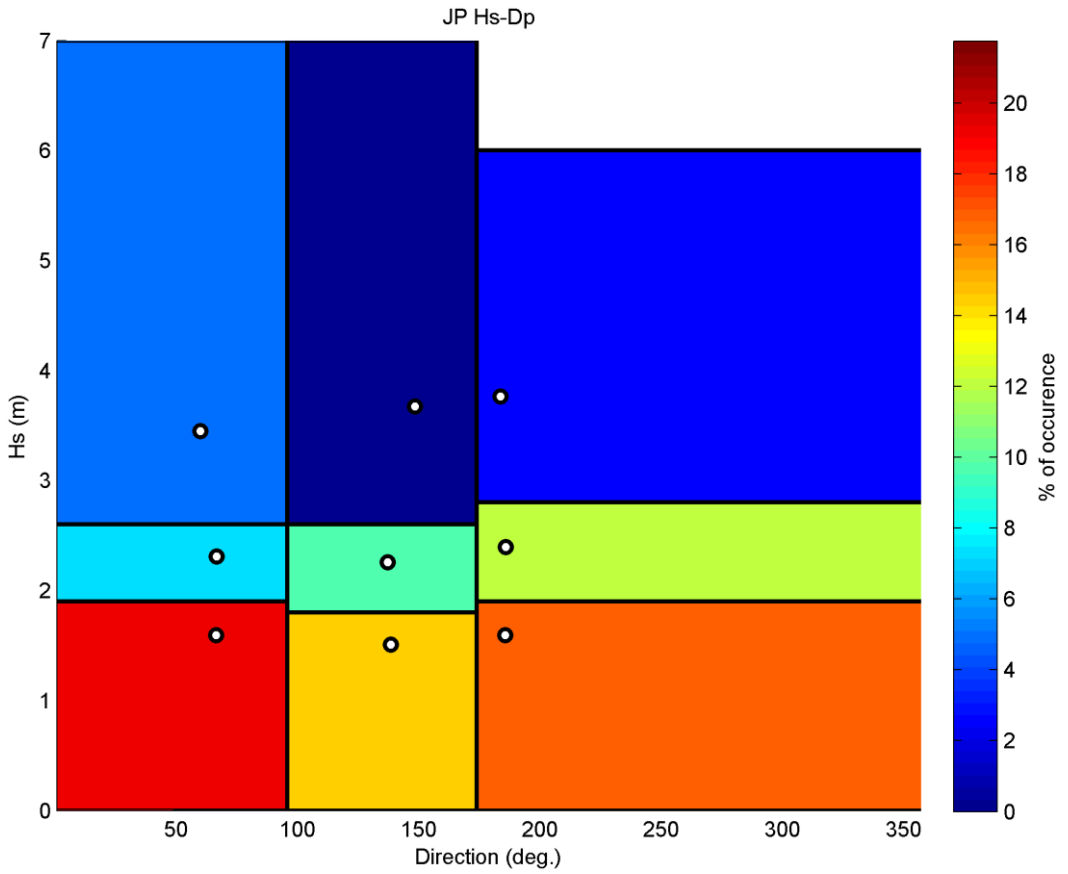


Figure 4.5 Reduced average annual wave climate based on the 10-year wave hindcast using 3 directional bins and 3 wave height bins (i.e. 9 wave classes). Colours indicate the probability of occurrence of a given class. The white dots are the representative wave condition of each wave class. The wave conditions are summarized in Table 4.3.

### 4.1.3. Residual current input reduction

In addition to the wave and tidal forcing, the effects of residual currents were included in the present model. Less guidance is available on the inclusion of additional forcing such as residual currents or winds to the input reduction approach (e.g. Lesser, et al., 2004).

The general residual current regime at the disposal site is dominated by longshore northwest or southeast-directed currents with magnitudes of up to ~0.3 $m.s^{-1}$ during peak events (see Figure 4.6). However, their repartition over the 10 year hindcast is very well balanced so that absolute net residual current magnitudes are very small (~1.0 $mm.s^{-1}$ towards the southeast). In the input reduction approach, the residual currents associated with each wave class were determined by averaging the residual current conditions associated with the wave events of each bin. The obtained representative conditions have small magnitudes and are directed predominantly towards the southeast or northwest quadrants (Table 4.2).

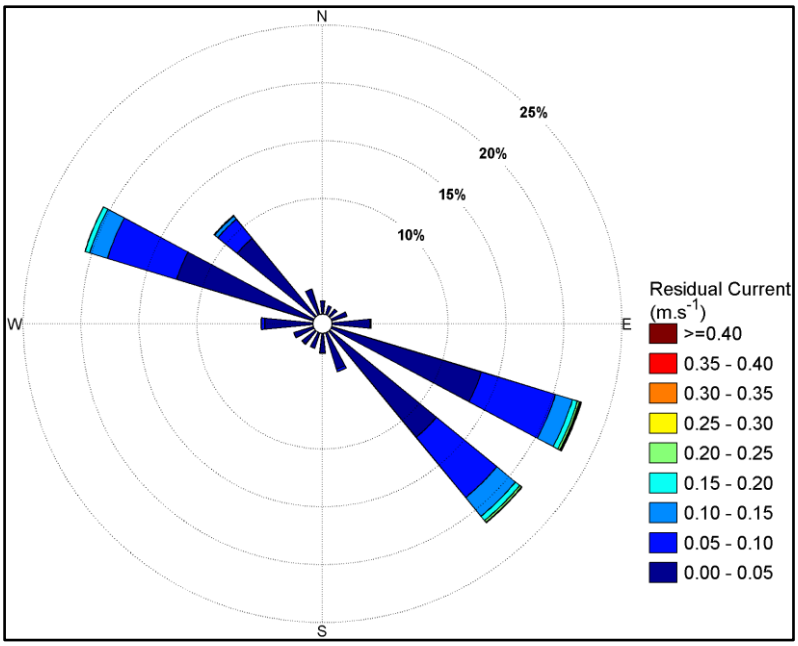


Figure 4.6 Residual current rose from the 10 year hindcast of residual (non-tidal) currents at the centre of the proposed disposal ground.

It is interesting to note that the two most energetic southerly wave events (classes 6 and 9, Figure 4.5) tend to be associated with northwest-directed net residuals while others show predominantly southeast-directed net residuals.

Despite these small residual net currents applied in the "reduced" morphological simulation, it is expected that discrete events with peak magnitudes could have significant impact on the sediment transport. Here these effects will be further investigated during discrete high energy events with opposing (i.e. southeast and northwest-directed) residual current flows. Note that high energy events are periods during which most of the sea bed changes will effectively occur due to the non-linearity of the sediment transport processes.

Table 4.2 Residual currents associated with each wave class.

| Wave class no. | Residual speed [cm.s$^{-1}$] | Residual direction [degT] |
|---|---|---|
| **1** | 0.29 | 259 |
| **2** | 0.73 | 115 |
| **3** | 3.93 | 121 |
| **4** | 1.11 | 128 |
| **5** | 1.59 | 129 |
| **6** | 0.58 | 237 |
| **7** | 1.54 | 131 |
| **8** | 1.88 | 138 |
| **9** | 1.97 | 269 |

### 4.1.4. Morphological acceleration factor

The morphological acceleration factor (morfac) is a technique to bridge the gap between hydrodynamic and morphological timescales (Lesser, G.R. et al., 2004). This technique consists of multiplying the calculated depth changes over a hydrodynamic time step $\Delta t_{hydrodynamic}$ by a constant factor $f_{MOR}$, effectively predicting morphological changes over a period:

$$\Delta t_{morphology} = \Delta t_{hydrodynamic} \cdot f_{MOR} \quad (3.4)$$

Such an approach obviously has limits and involves many implicit assumptions. However it has been successfully applied on many studies to estimate medium-term morphological evolutions of tidal (e.g. Van der Wegan and Roelvink, 2008) and mixed tide and wave environments (e.g. (Grunnet, et al., 2004; Lesser, 2009; Reniers et al., 2004). This acceleration method was combined with the reduced residual, tide and wave forcing outlined above to simulate the morphological evolution of the study area over an annual period (i.e. 365 days).

To account for the random phasing between waves and tides that occurs naturally, each of the representative wave conditions was simulated for the duration of one complete tidal cycle. A morphological acceleration factor specific to each wave class was defined so that the morphological duration of the wave class matches its probability of occurrence within the period considered. The morphological factor is computed following.

$$f_{MOR} = \frac{p_j \cdot Period\ Duration}{T_{morph\ tide}} \quad (3.5)$$

where $p_j$ is the probability of occurrence of wave conditions falling in the wave class (or bin) j (e.g. Figure 4.5), “Period Duration” is the total duration to be simulated, and $T_{morph\ tide}$ is the duration of the representative morphological tide. The wave climate reduction and associated morfacs obtained for a 1-year simulation based on the average annual wave climate are provided in Table 4.3. Morfacs range from 20 to 150 for high to low wave energy events, respectively.

The model system is run for each different wave class forcing, one after the other, over a complete tidal cycle using the appropriate morphological factor. The final bathymetry of each wave class simulation is used as the initial bathymetry for the next simulation. Running each wave class separately rather than using time-varying wave forcing and morfacs over a single continuous simulation suppresses any risk of discontinuities that can potentially develop in suspended sediment concentrations when the morfacs are changed after a given wave class simulation (see Lesser, 2009).

Table 4.3 Wave classification and associated morphological factors for a 1 year period, based on an average annual wave climate defined from the 10-year hindcast.

| Wave class no. | Representative Hs (m) | Representative Tp (sec) | Representative direction (deg.) | Probability of occurrence (%) | Morfac equivalent 1 year |
|---|---|---|---|---|---|
| **1** | 1.59 | 8.94 | 66.55 | 0.22 | 152.46 |
| **2** | 2.31 | 9.69 | 66.68 | 0.08 | 53.66 |
| **3** | 3.45 | 9.74 | 59.89 | 0.04 | 25.19 |
| **4** | 1.51 | 10.23 | 138.47 | 0.21 | 150.42 |
| **5** | 2.26 | 11.12 | 137.30 | 0.09 | 63.37 |
| **6** | 3.68 | 11.99 | 148.50 | 0.03 | 19.76 |
| **7** | 1.59 | 11.48 | 185.78 | 0.22 | 151.23 |
| **8** | 2.40 | 11.55 | 185.97 | 0.09 | 63.59 |
| **9** | 3.76 | 11.67 | 183.68 | 0.03 | 21.13 |

### 4.1.5. Suitability of the technique for the project location

Presently there is not generic approach to correctly reproducing all features of a coastal systems morphological behaviour over a medium (months to year) time-frame within a numerical model framework.

To address this limitation a reduction strategy, optimised for a given study objective (De Vriend, et al., 1993; Lesser, 2009), can be used to provide guidance on what the salient processes or features that need to be conserved within the modelling system are and what simplifications ca be made.

The reduction techniques (outlined in 4.1.1 and 4.1.4) involves many implicit assumptions, which inevitably introduce errors in the estimates of morphological evolution. The technique need to be optimised for a given study objective and the assumptions need to be considered when assessing the results for a specific site or time-scale of interest.

The objective of the present study is to establish a model that can qualitatively simulate the fate of the dredged sediment deposited within the disposal ground. The key sediment transport drivers over an annual basis are expected to be wave, tidal and residual current forcing. Of the three processes, wave induced entrainment and transport (due to wave orbital asymmetry) is expected to be the salient process at the disposal ground.

The interaction of the ambient wave-driven transport with the tidal oscillations becomes significant near the harbour entrance and needs to be retained as well. This is achieved by considering a single morphologically representative tide that considers the range of spring and neap tidal forcings and their non-linearity (see 4.1.1). The spring-neap oscillations are not expected to significantly modify the general sediment transport and morphological change patterns but rather modulate their magnitudes.

Net residual current velocities are small in the long term and are expected to have a limited net effect on the dispersion of sediment. Conversely, discrete events have the potential to enhance wave induced entrainment and transport mechanisms, while increased occurrences of residual currents with a specific direction over a defined time-period could modify the general sediment transport dispersion. The effect of these larger residual current events is examined by modelling discrete events with high wave energy and peak residual currents from key directions; supplementing the longer term net transport modelling addressed by the reduction technique.

Winds are not directly included in the present approach as they are not expected to be directly significant in the context of the annual sub-tidal sediment transport regime. However, the study site is exposed to local wave generation from the fetch area to the north as well as local wind-driven currents. These features are taken into account through the wave and hydrodynamic forcing as they are defined from hindcast simulations that explicitly include wind effects.

In terms of temporal scale, it is assumed that a reduced wave climate reproducing the annual potential for sediment transport should be suitable to assess morphological impacts with respect to the fate of the disposed sediment. Therefore a representative annual wave climate was used to force the model and no particular season separation was considered. Further, as we are mainly concerned with reproducing the cumulative effects of discrete

events on the medium term morphological evolution, the event chronology was not expected to be of critical importance. The sequence of wave classes within a complete simulation was thus randomly assigned, with each condition being simulated once, rather than trying to reproduce a realistic wave climate history as a combination of successive representative classes (e.g. Walstra et al., 2013).

## 4.2. Real-time simulations

The accelerated morphological simulations were supplemented by real-time simulations of two high wave energy events with large residual current magnitudes and opposing directions (i.e. northwest directed and southeast-directed). Both events took place in 2010 and had an offshore significant wave height approaching 2 m and residual current magnitudes stronger than 0.15 $m.s^{-1}$. The simulations were run for 4 days centred on the peak conditions experienced during the events (Table 4.4).

These simulations allowed investigation of detailed real-time variations in sediment transport patterns due to different wave and residual current forcing that cannot be fully reproduced by a reduced model configuration. These simulations also provided a basis to verify the reduced models overall robustness in terms of predicted net transport patterns and morphology.

For the two real events simulated, tidal and residual currents and 2D wave spectra boundary conditions were fully nested from the regional wave and current hindcast models described in Section 2.2 and 2.3.

Comparisons between the Delft3D predicted wave and current characteristics and those from the relatively coarser boundary sources (SWAN and ROMS for the waves and currents respectively) at a site within the proposed disposal ground are given in Figure 3.7-Figure 3.10 and show good agreement between ROMS and Delft3D-flow and SWAN and Delft3D-Wave for both events considered.

Table 4.4 Wave and residual current conditions during modelled events.

| | **Northwest residual current event** | **Southeast residual current event** |
|---|---|---|
| **Start Time** | 24-May-2010 00:00 | 25-Dec-2010 00:00 |
| **End Time** | 28-May-2010 00:00 | 29-Dec-2010 00:00 |
| | **Conditions during flow peak** | |
| **Hs [m]** | 1.9 | 1.7 |
| **Dp [deg. From]** | 70 | 45 |
| **Residual Current Speed [m/s]** | 0.17 | 0.22 |
| **Residual Current Direction [deg. To]** | 300 | 110 |

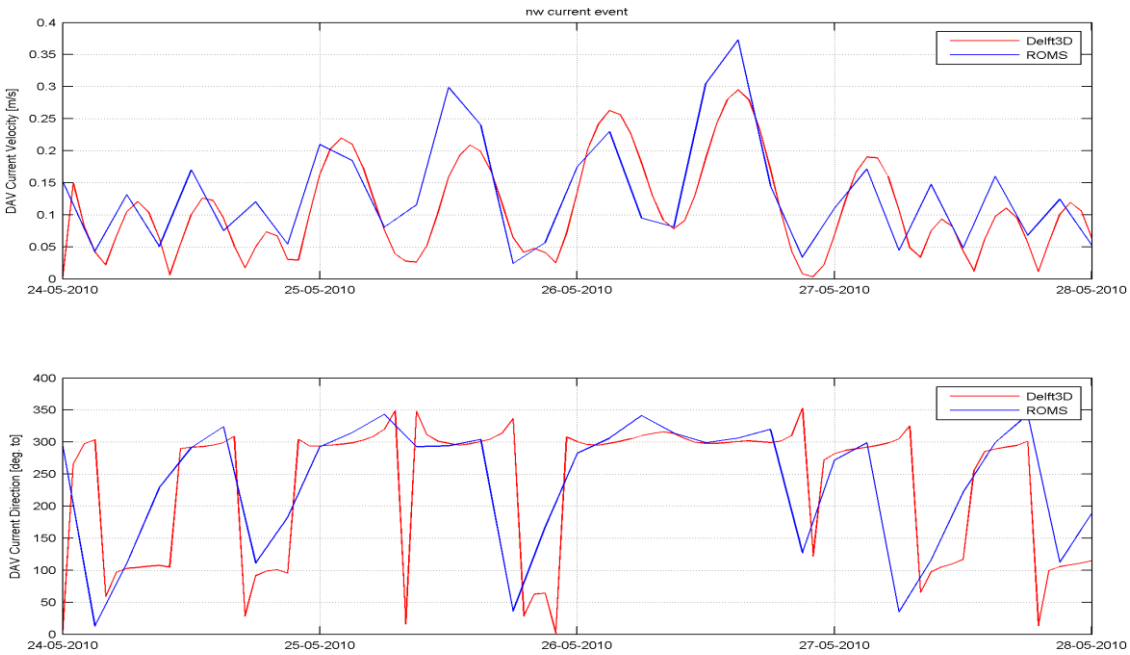


Figure 4.7 Predicted depth average currents predicted by both Delft3D-Flow and ROMS at the proposed capital disposal site during a predominant NW event

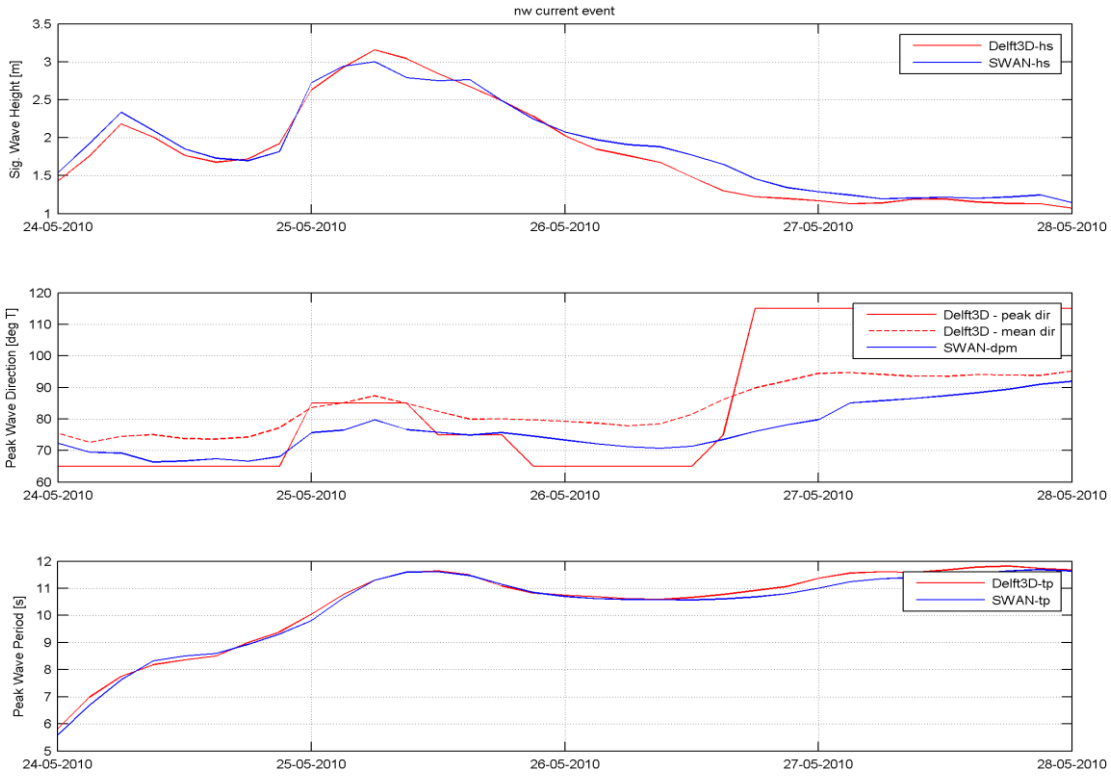


Figure 4.8 Predicted Significant wave height, peak wave direction and peak period predicted by both Delft3D-Wave and SWAN at the proposed capital disposal site during a predominant NW event

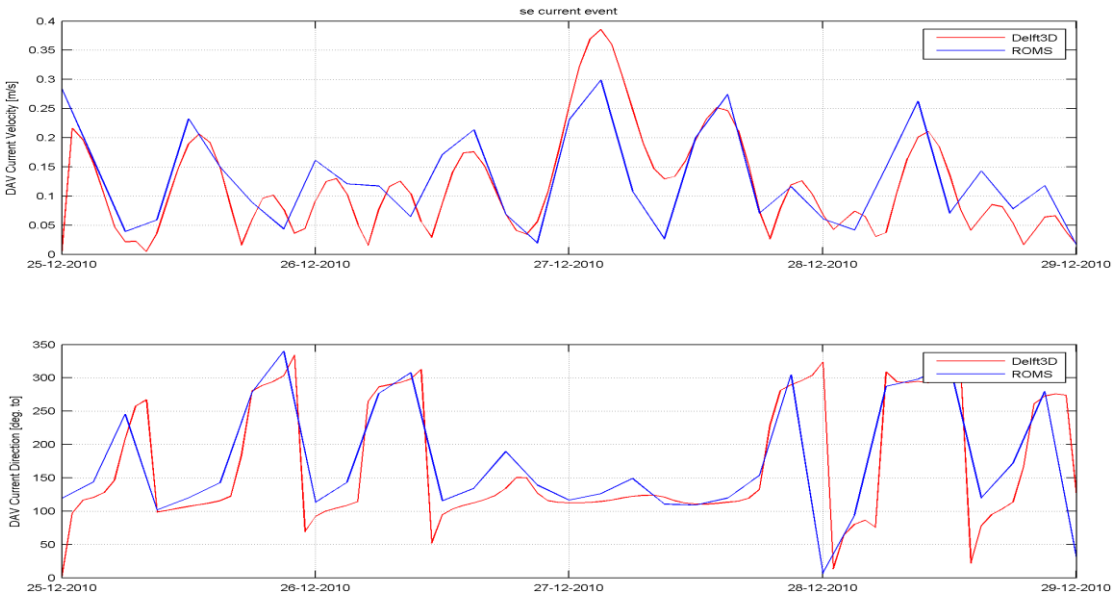


Figure 4.9 Predicted depth average currents predicted by both Delft3D-Flow and ROMS at the proposed capital disposal site during a predominant SE event

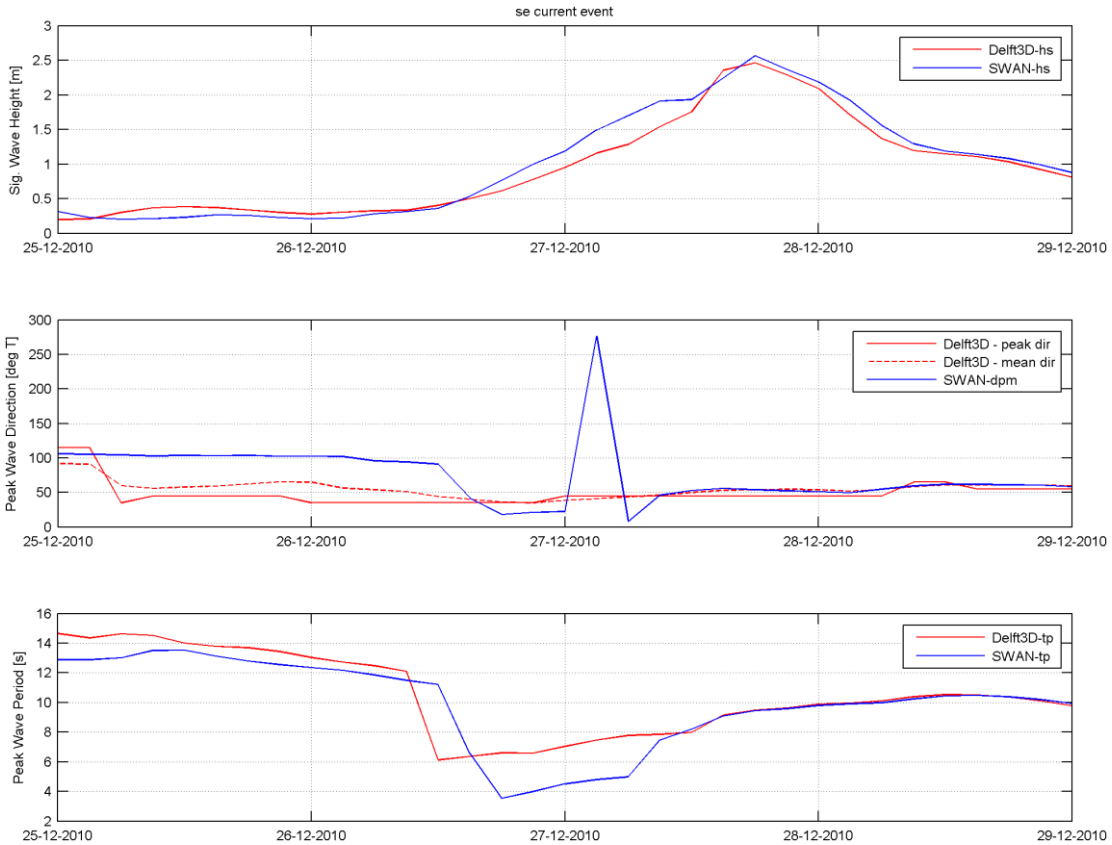


Figure 4.10 Predicted Significant wave height, peak wave direction and peak period predicted by both Delft3D-Wave and SWAN at the proposed capital disposal site during a predominant SE event

# 5. RESULTS

## 5.1. Annual morphological simulations

To investigate the morphological changes expected following the discharging of dredge spoil at the disposal ground, annual morphological simulations were undertaken using an input reduction average wave climate (Table 4.3). The approach provides a reasonable picture of the net sediment dispersion footprint around the mound on an annual basis. The instantaneous system response to discrete events with different forcing conditions is further outlined in section 4.2.

To isolate the effect of dredged sediment discharged of at the disposal ground, the initial model conditions assumed sediment available only within the disposal ground, which is then progressively dispersed throughout the sequence of representative events.

Model predicted circulation, wave and sediment dynamics for the most energetic annual wave climate events (i.e. events 3, 6 and 9, Table 4.3) are presented in Figure 5.1 to Figure 5.3.

The ambient wave energy at the disposal site varies depending on the offshore incident wave direction on the continental shelf, with the comparatively frequent southerly swell events needing to refract around Banks Peninsula to reach the proposed disposal site; resulting in significant wave height reduction (see Figure 5.3). Wave refraction is also required to propagate southeast wave event into the disposal site, while wave events from the northeast propagate more directly into the disposal site.

Key features of the annual morphological simulations include;

- The magnitude of the net circulation and sediment transport fields are proportional to the disposal sites exposure to wave energy.
- The general circulation pattern consists of a predominant northwest directed flow through the eastern half of the domain, veering slightly more northward in the more western half of the domain. This deviation is more significant during the northeast event.
- During the south and southeast wave events (Figure 5.2 and Figure 5.3), some easterly return flows develop along the coast, east of the harbour entrance, while a northwest-directed longshore flow is forced west of the entrance.
- Nearshore flows are more variable and generally an order of magnitude larger during the northeast event, with an offshore directed component developing west of the harbour entrance (Figure 5.1).

For these energetic wave events, the sediment within the disposal ground is mobilized and transported, with suspended transport fluxes (pathways) consistently directed toward the west-northwest, with magnitudes and directions strongly modulated by the ambient wave energy level.

Sediment transported at some distance from the disposal ground indicates a potential re-mobilisation of the sediment that was previously transported out

of the disposal site, and subsequent transport by wave and current processes (e.g. Figure 5.1). These transport processes could potentially result in recirculation of the sediment into the channel region or Harbour depending on the instantaneous flow patterns. This is expected to be a secondary process that will apply only to a relatively small amount of sediment.

The total morphological changes at the completion of the annual morphological simulation are shown in Figure 5.4. The model predicts sediment mobilization throughout the entire disposal ground with a sediment spreading pattern that is skewed towards the west, consistent with the wave general wave field vectors and induced shear stress within the disposal ground.

The schematic residual current climate applied in the simulation, which is mostly south-eastward (Table 4.2), as well at the underlying tidal ellipse (Figure 4.1) are peripheral in terms of the annual morphological response of the disposed sediment compared to the wave processes.

In order to provide a picture of the longer term morphological changes expected in the vicinity of the disposal ground, the model was run over a 5 year period from 2007 to 2011 (included). The wave and residual current climates of each year were reduced to a set of representative classes as outlined in section 3.1.2 to reproduce the inter-annual forcing variability. The cumulative morphological changes of the post-disposal bathymetry over the 5-year periods are presented in Figure 5.5.

Key features of the inter-annual morphological simulations include;

- Sediment is expected to be mobilised throughout the entire ground and the model predicts erosion of the entire sediment volume initially placed in the disposal ground by the end of the 5-year period (1.44 m thickness, see Figure 5.6 for details of the erosion patterns).

- The sediment migration direction is consistently towards the west.

- The sediment spreading pattern after the 1 year (2007) is very similar to that of the average annual climate predictions (Figure 5.4).

- Predictions for the subsequent years show continued erosion from the disposal ground region as well as mobilization of the sediment that previously migrated from the ground.

- The initial sediment volume is progressively spread over increasingly large areas.

- A fraction of that sediment moves out of the model domain to the west while another small amount reach the nearshore zone but predicted sediment thicknesses eventually become insignificant by the end of the 5-year period.

The sequence of the morphological changes for the 5-year period suggests that the shipping channel may indeed be relatively sheltered from the main sediment migration footprint with a deposition pattern skewed more westwards than south-westward.

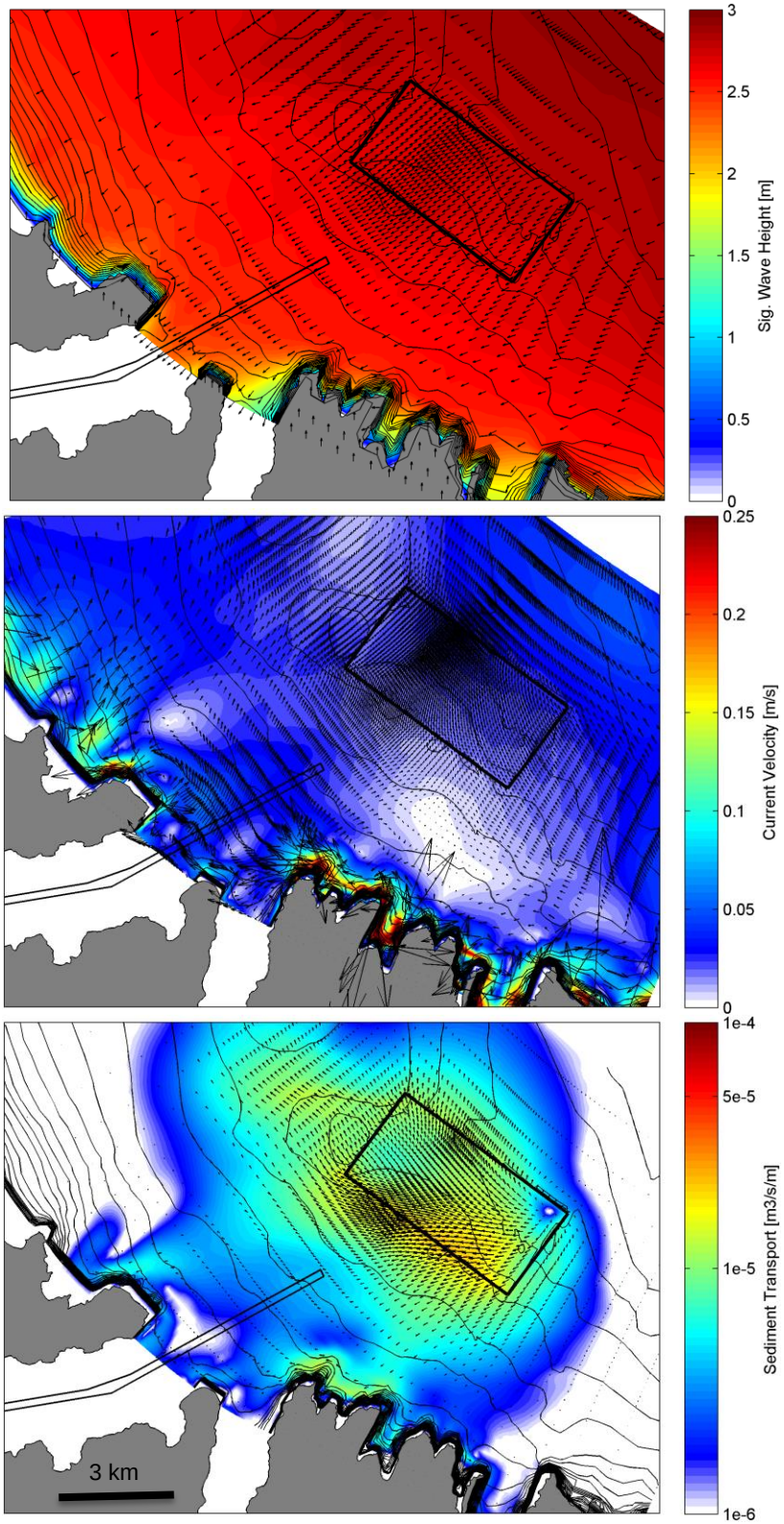


Figure 5.1 Wave, circulation, and sediment transport fields averaged over the representative tide for Event 3 of Table 3.3, over the post-disposal bathymetry. All colour and quiver scales are equal in Figures 4.1, 4.2 and 4.3 for comparison. Note a logarithmic colour scale is used for the sediment transport field.

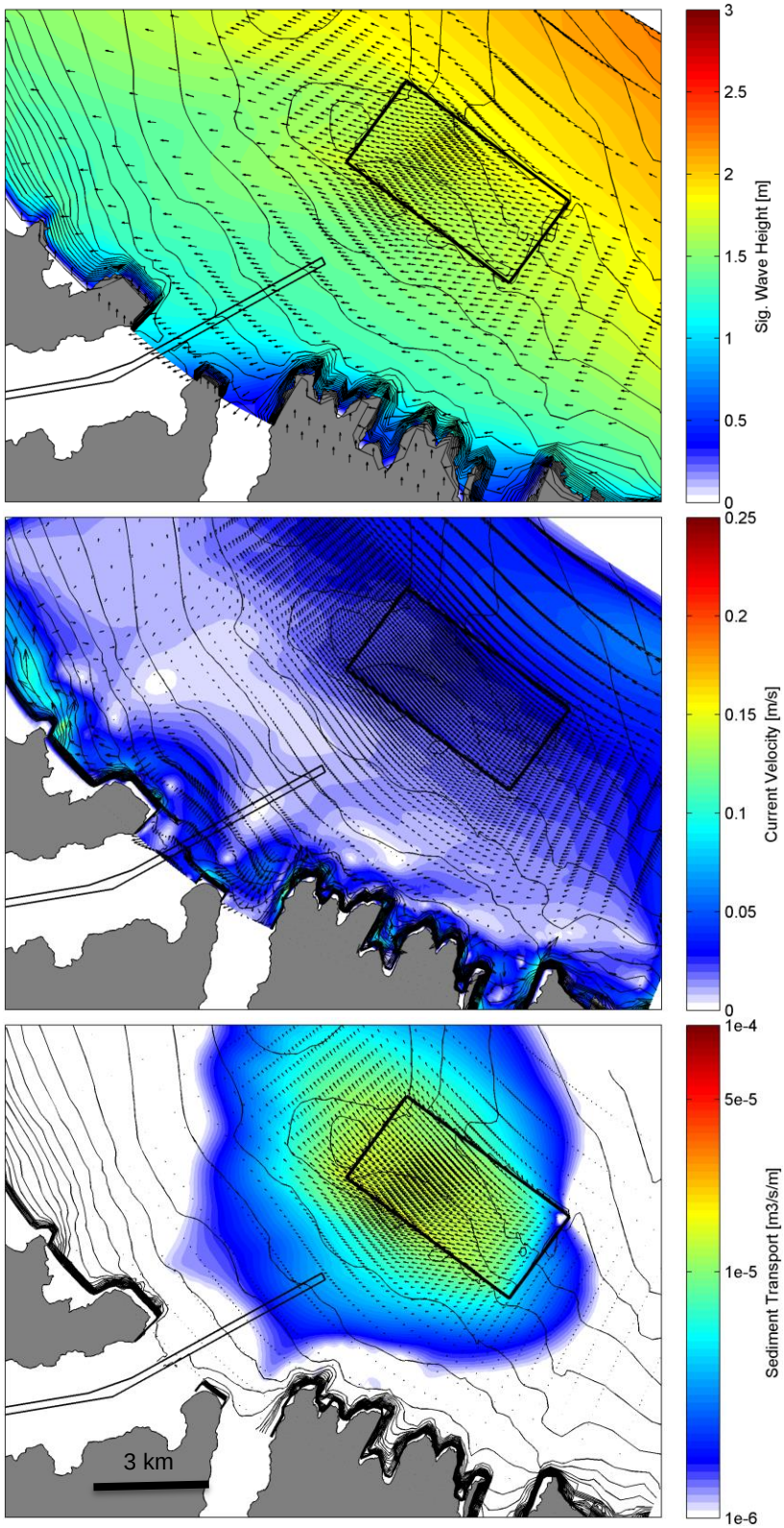


Figure 5.2 Wave, circulation, and sediment transport fields averaged over the representative tide for Event 6 of Table 3.3, over the post-disposal bathymetry. All colour and quiver scales are equal in Figures 4.1, 4.2 and 4.3 for comparison. Note a logarithmic colour scale is used for the sediment transport field.

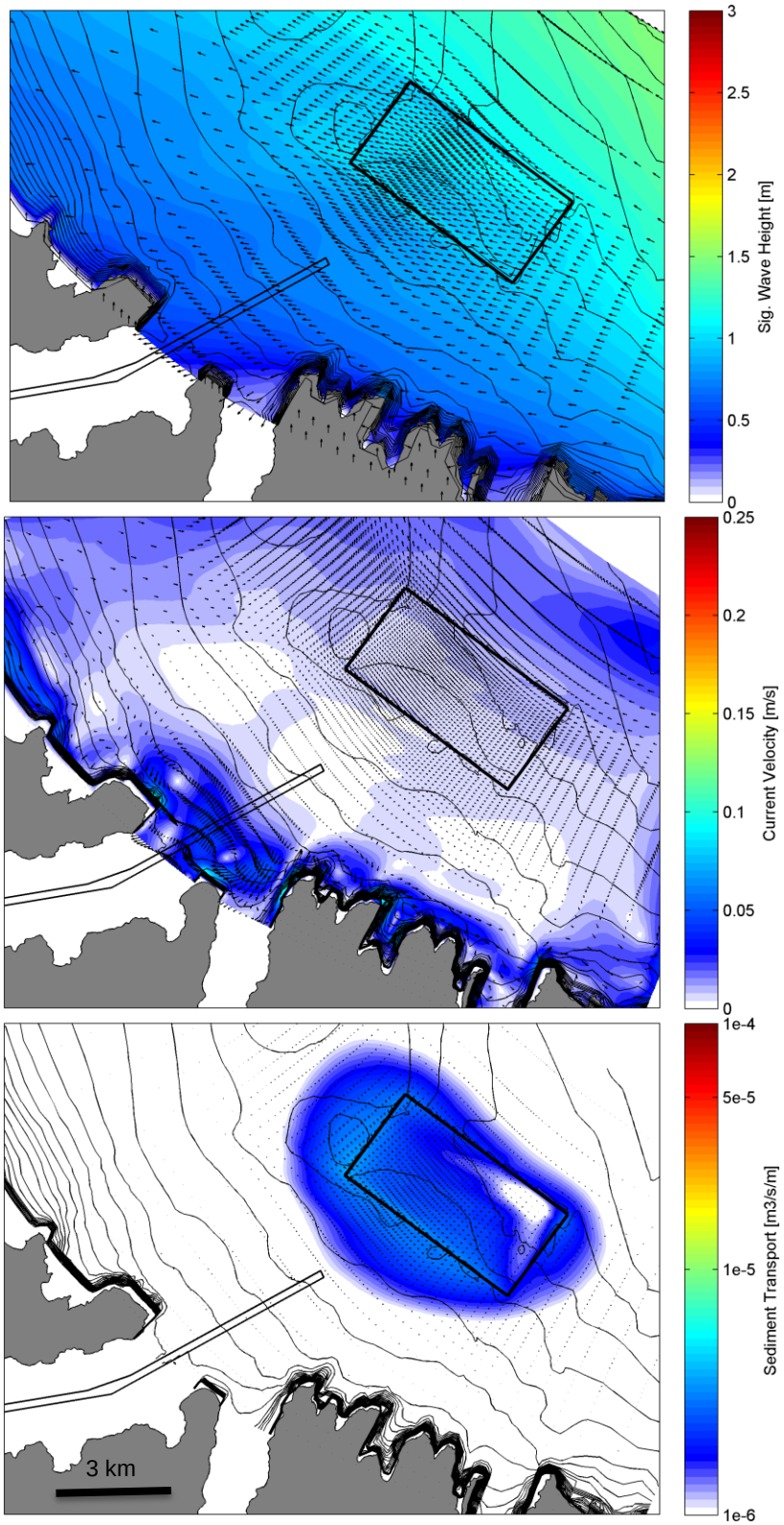


Figure 5.3 Wave, circulation, and sediment transport fields averaged over the representative tide for Event 9 of Table 3.3, over the post-disposal bathymetry. All colour and quiver scales are equal in Figures 4.1, 4.2 and 4.3 for comparison. Note a logarithmic colour scale is used for the sediment transport field.

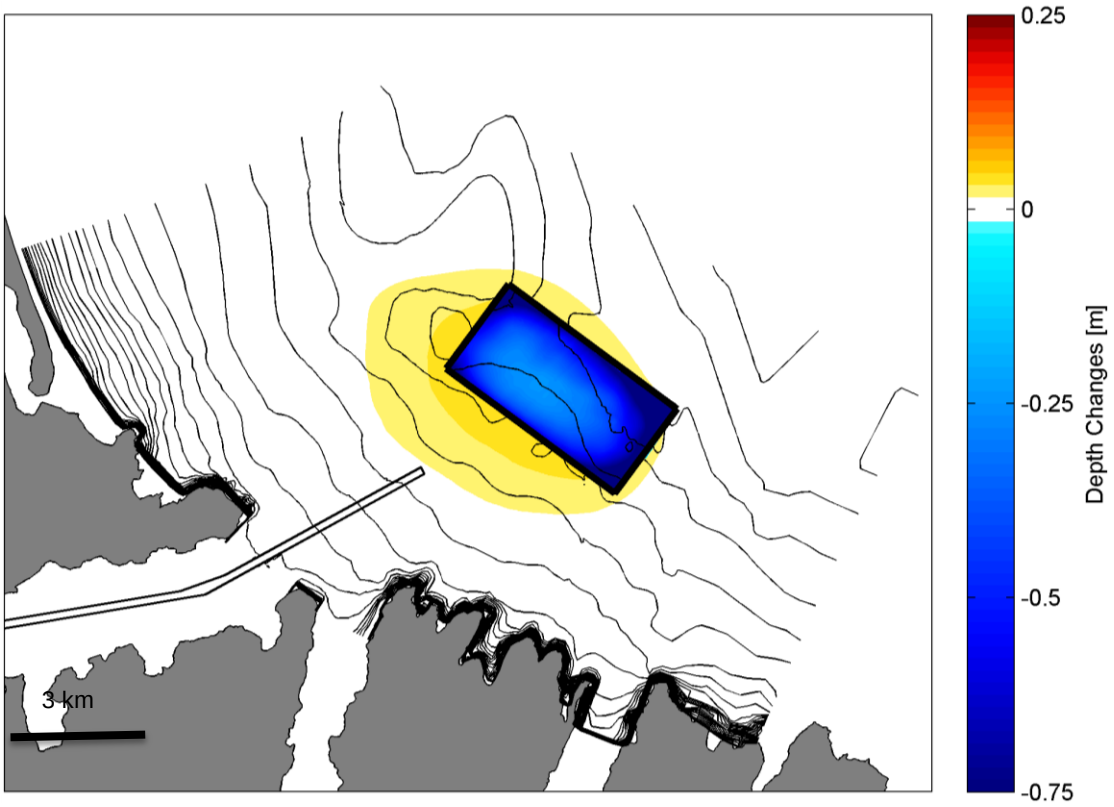


Figure 5.4 Morphological changes predicted after 1 year. The initial post-disposal bathymetry was obtained by adding 1.44 m of sediment throughout the entire ground (~12.5 $km^2$), equivalent to the 18 million $m^3$ sediment. Initial bathymetric contours are shown in black. A positive magnitude indicates sedimentation.

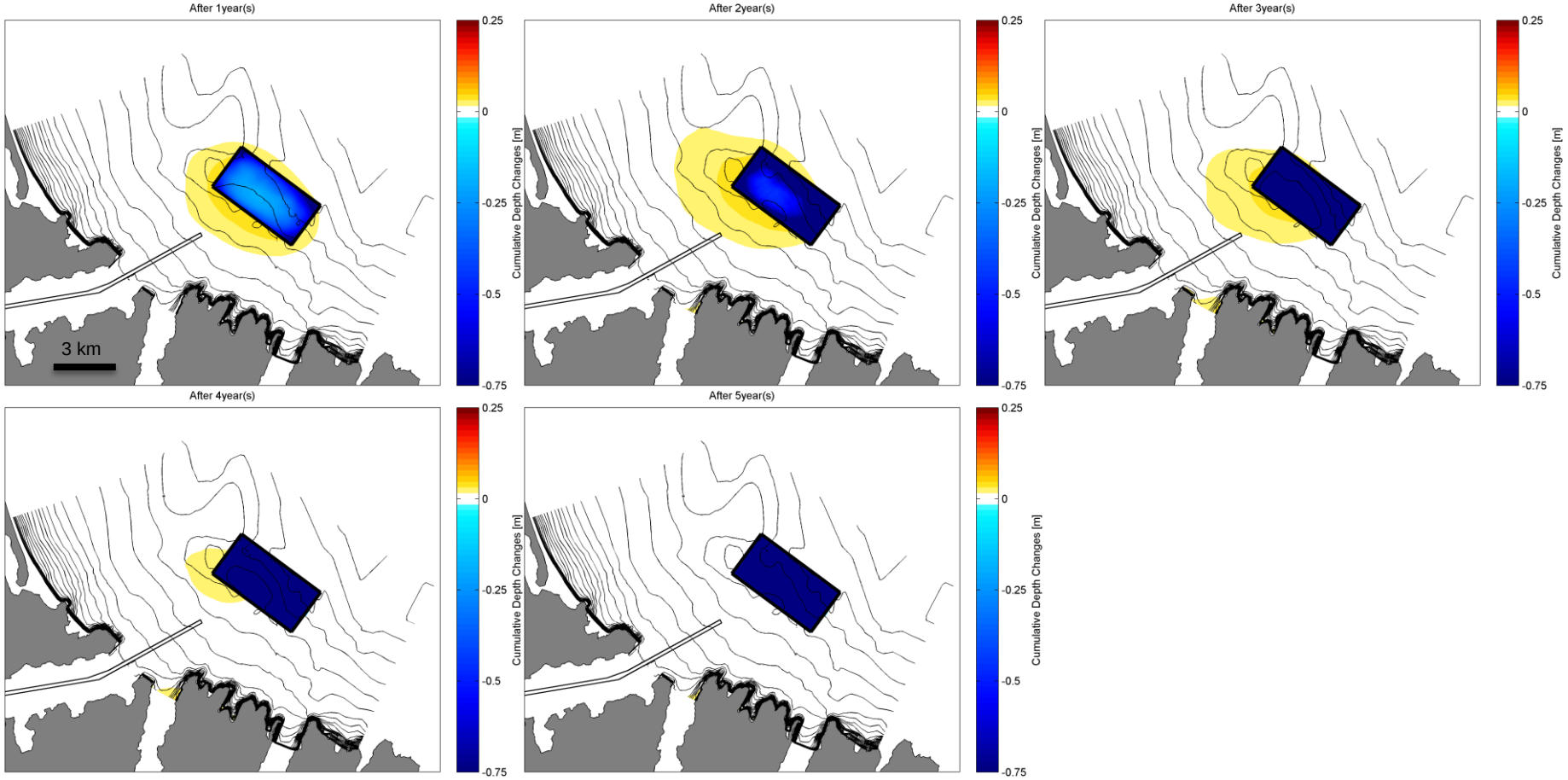


Figure 5.5 Cumulative morphological changes after each year over a 5-year morphological simulation of the disposal ground. The initial post-disposal bathymetry was obtained by adding 1.44 m of sediment throughout the entire ground (~12.5 $km^2$), equivalent to the 18 million $m^3$ sediment. Initial bathymetric contours are shown in black. A positive magnitude indicates sedimentation.

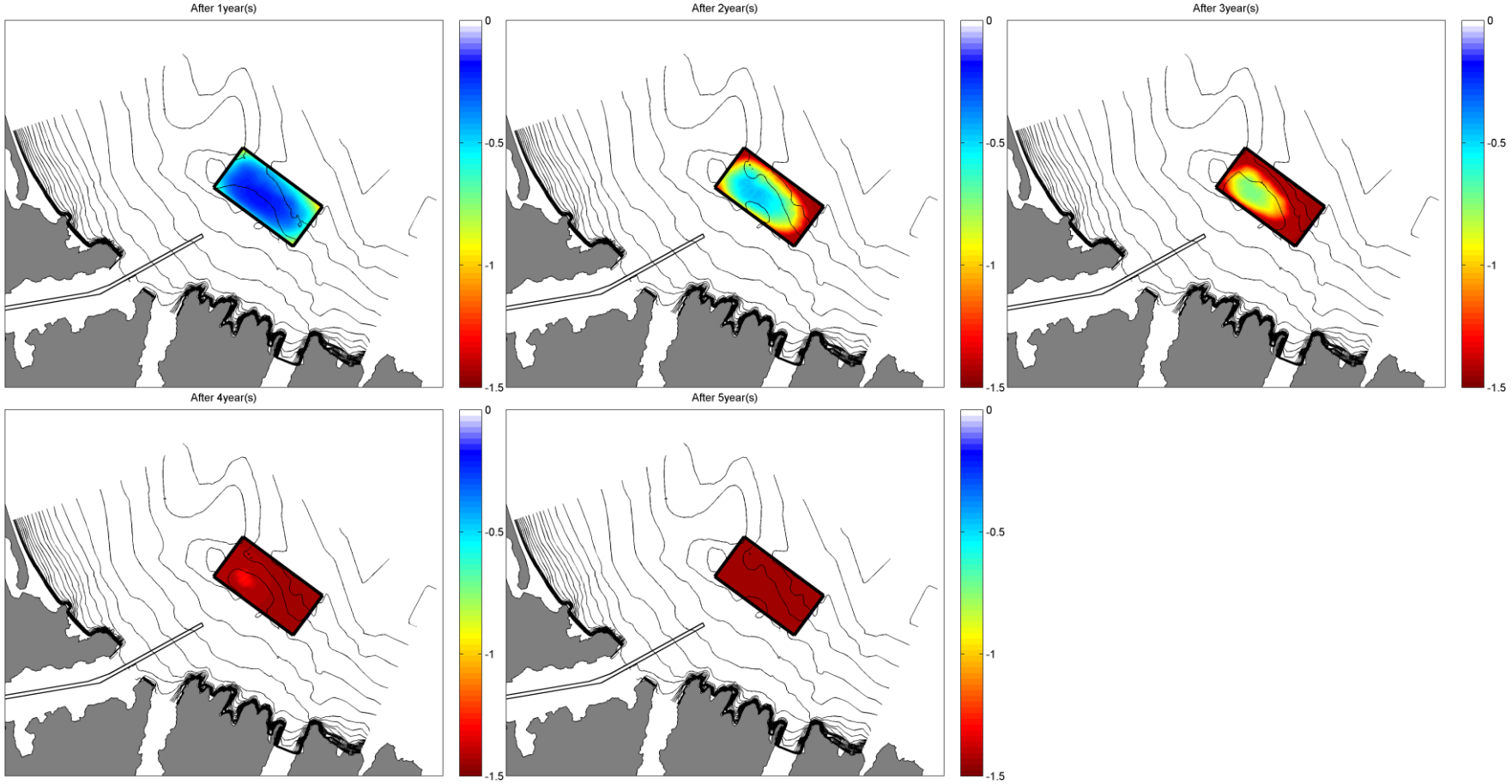


Figure 5.6 Cumulative erosion patterns of the sediment volume initially present in the disposal ground. The initial post-disposal bathymetry was obtained by adding 1.44 m of sediment throughout the entire ground (~12.5 $km^2$), equivalent to the 18 million $m^3$ sediment. Initial bathymetric contours are shown in black. A positive magnitude indicates sedimentation. Note the associated sedimentation patterns visible in Figure 5.5 are not reproduced here due to the different colour scale range.

## 5.2. Real-time simulations results

The simulations of two real events with large waves and residual current velocities supplement the long term simulation results to provide a picture of the detailed wave, circulation and sediment transport patterns that develop during energetic events. These types of events are expected to be responsible for the most significant morphological changes due to the non-linearity of sediment transport processes and resulting morphological adjustments.

At the site, the residual circulation regime is mostly bi-modal, dominated by events with either northwest or southeast-directed currents (see Figure 4.6), so two events with these opposing residual current directions were identified in the hindcast wave and current climates for the real time simulations. Respective time-series of wave and current conditions at the centre of the ground are shown in Figure 5.7 and Figure 5.8 for the southeast and northwest residual current events respectively. Both events were initialized with a post-disposal bathymetry, and assuming a homogenous spreading of sediment to be dredged throughout the ground.

It is stressed that the situations modelled are conservative, since in theory the sediment volume will be progressively disposed of at the site over potentially two dredging campaigns spanning 9-14 months each, and the discharged sediment is also expected to be continually dispersed over time dredging campaign period.

While the absolute magnitudes of the predicted morphological changes should be interpreted with care since no quantitative validation of the sediment transport model was possible, the predicted patterns of changes are considered to be valid.

### 5.2.1. Northwest residual currents

Circulation, sediment transport, and wave fields predicted during the peak conditions of the event for the existing and post-depositional bathymetries under northwest-directed events are shown in Figure 5.9.

For the event modelled, the ambient flow is predominantly towards the northwest, with velocity of ~0.20 $m.s^{-1}$ throughout the disposal ground (Figure 5.9, middle). The combination of residual currents and wave orbital velocities mobilises sediment over the entire ground, with increased transport flux magnitudes over the relatively shallower south-western half of the disposal ground as the combined flow accelerates (Figure 5.9, middle).

The decreased depths within the disposal ground result in enhanced interactions with incident waves, which will increase the ambient bed shear stress levels and in turn enhance the potential for sediment mobilisation and transport. The effect of shallower depths on the wave height and bed shear stress fields within the spoil ground due to the disposal of sediment is illustrated in Figure 5.10.

For this event, the shallower disposal ground results in a wave height increase of ~10 cm in the lee of the disposal ground, particular notably toward Godley Heads. This corresponds to an increase of the maximum bed shear stresses by up to 0.4 $N.m^{-2}$ within the disposal ground.

Morphological changes over the event (Figure 5.11) indicate a clear westwards migration of the disposed sediment.

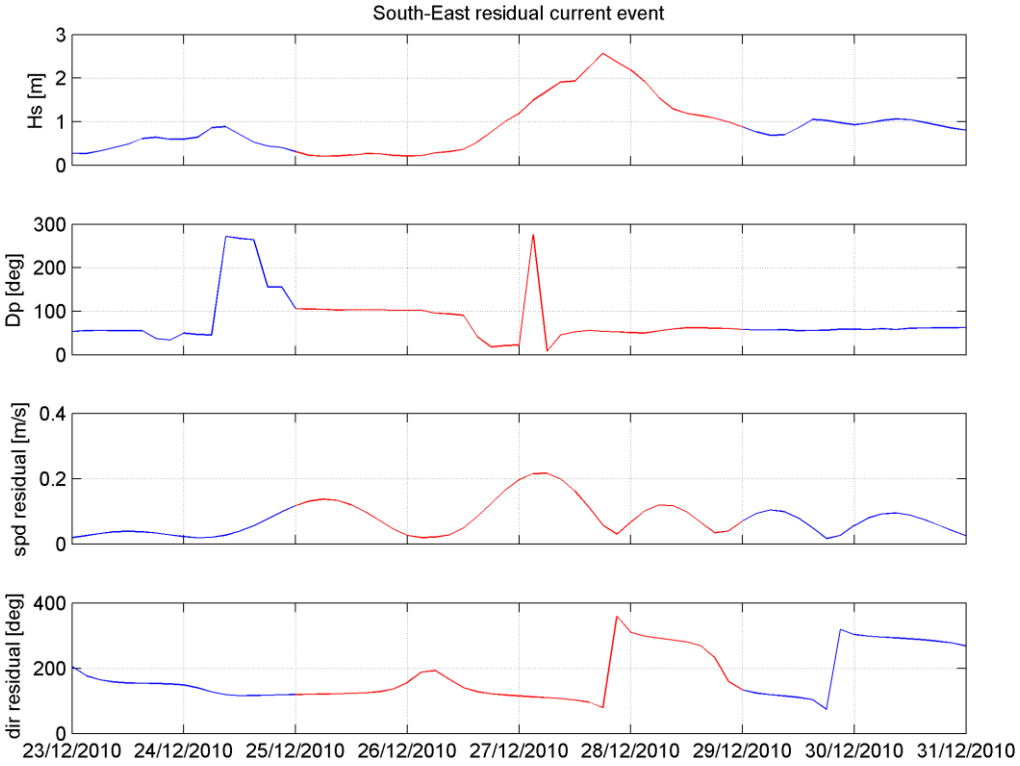


Figure 5.7 Wave conditions and residual currents at the centre of the disposal ground during the event with southeast-directed residual current. The simulation period is shown in red.

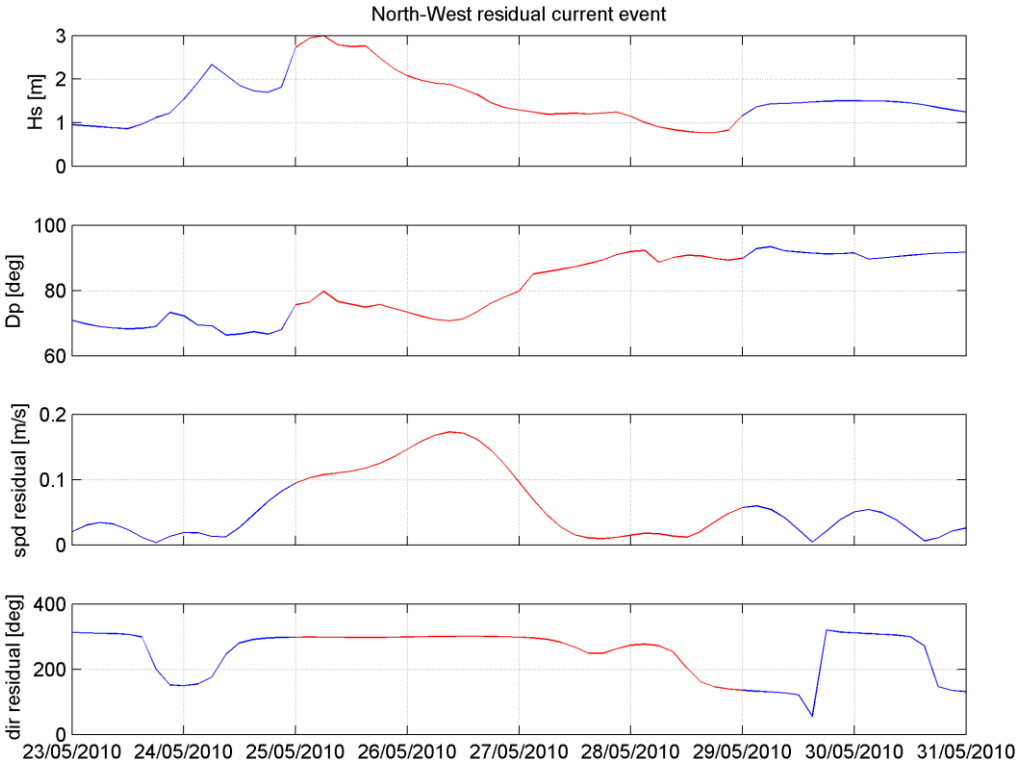


Figure 5.8 Wave conditions and residual currents at the centre of the disposal ground during the event with northwest-directed residual current. The simulation period is shown in red.

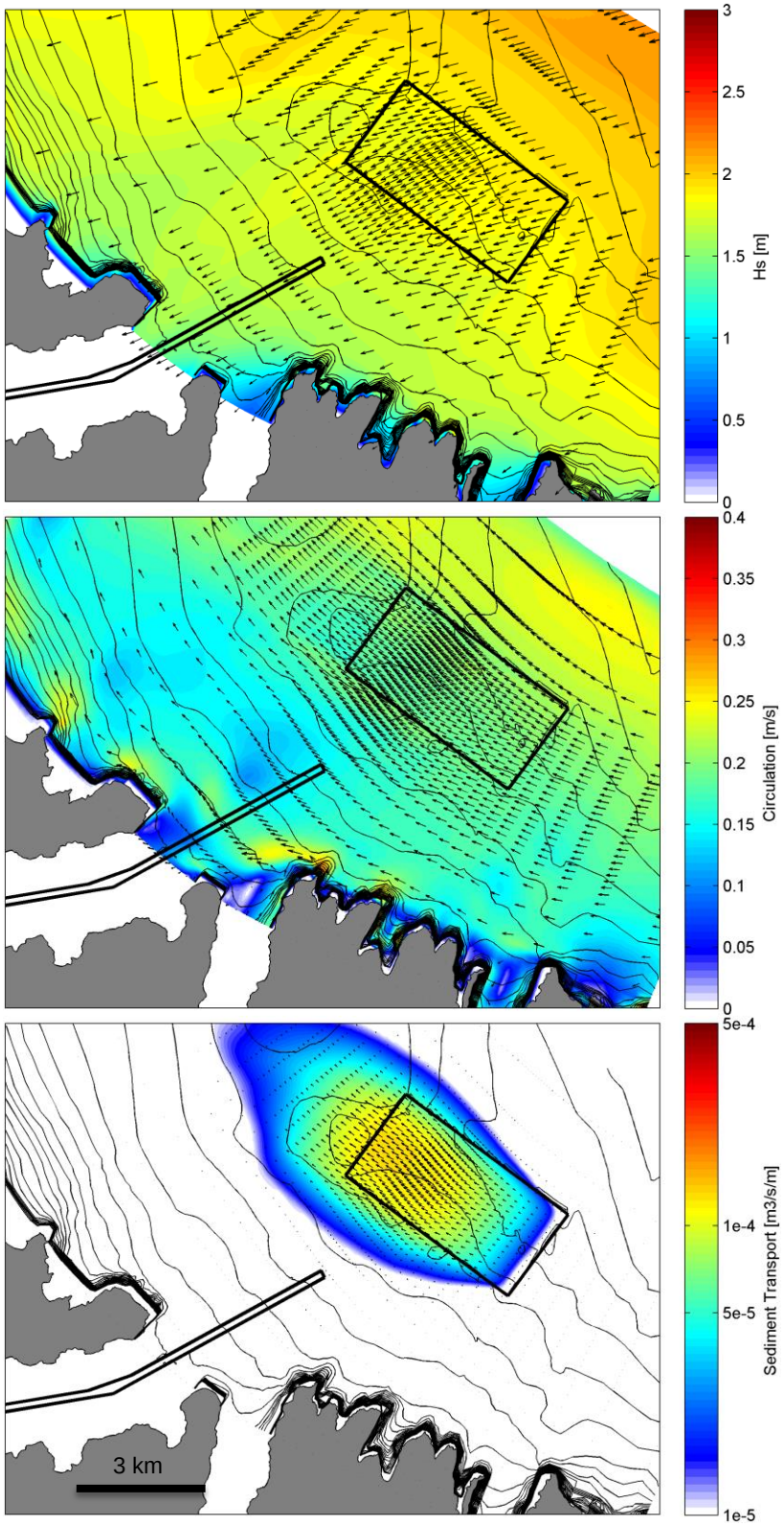


Figure 5.9 Wave, circulation and sediment transport fields during northwest-directed residual currents over the post disposal bathymetry. Note a logarithmic colour scale is used for the sediment transport field.

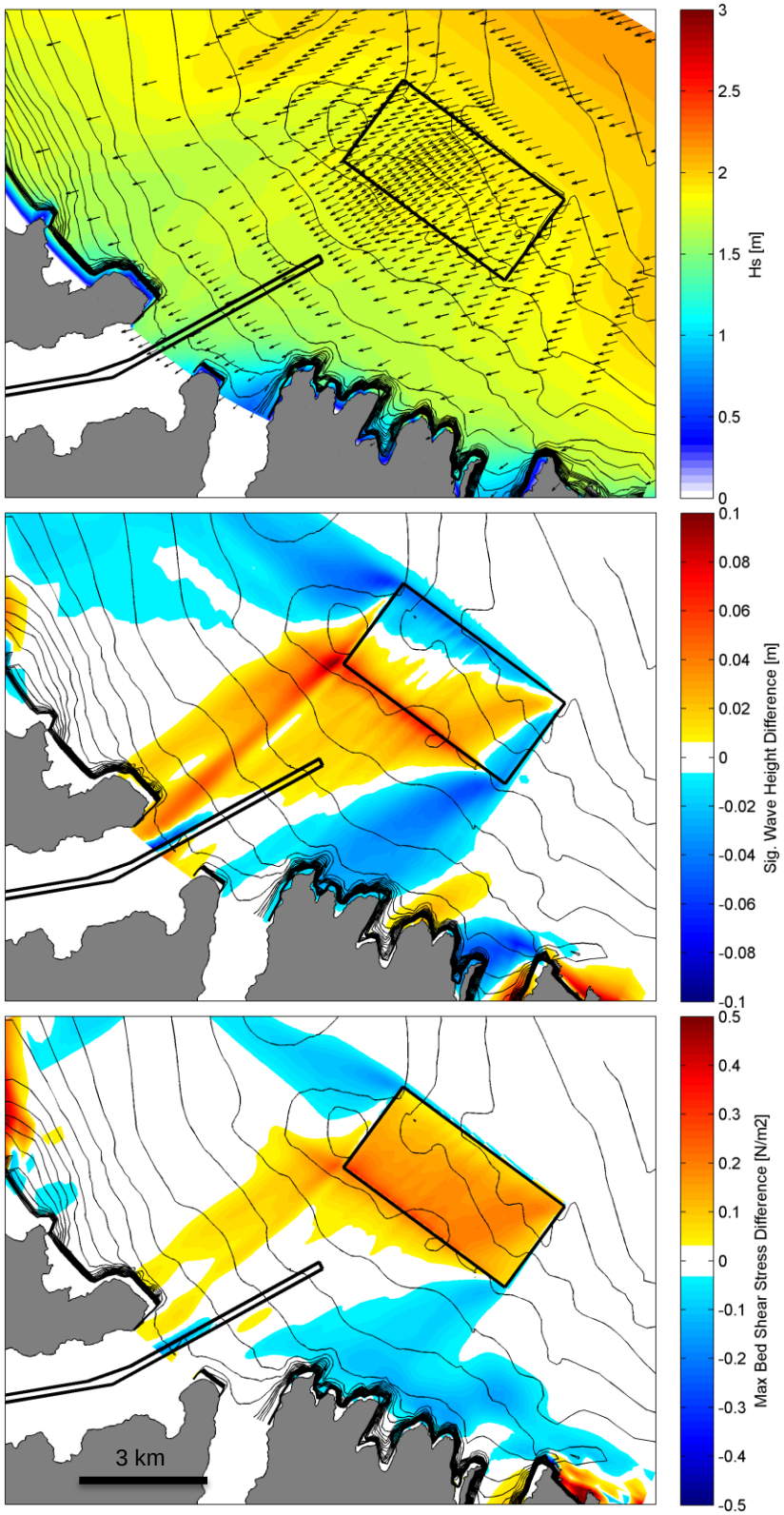


Figure 5.10 Significant wave height field over the post disposal bathymetry (top) and associated differences in significant wave height (middle) and maximum critical shear stress (bottom) relative to the existing state during the event with northwest -directed residual currents.

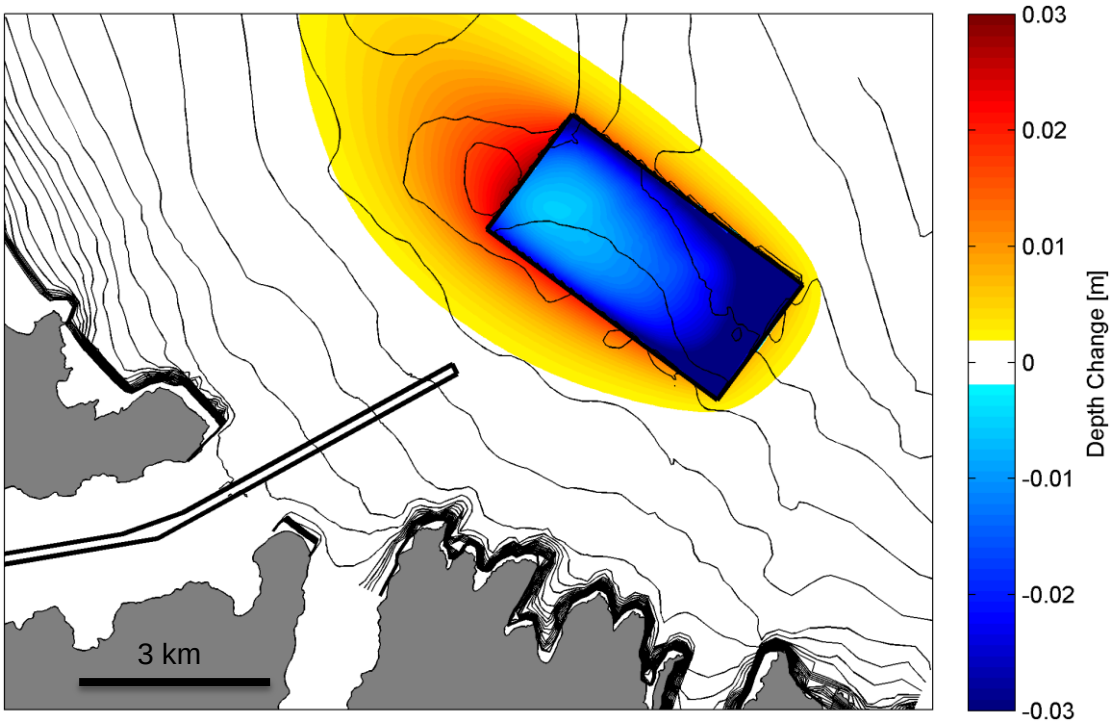


Figure 5.11 Morphological changes predicted at the end of the 4-day event with northwest-directed residual currents. A positive magnitude indicates sedimentation.

### 5.2.2. Southeast residual currents

Circulation, sediment transport, and wave fields predicted during the peak conditions of the event with southeast-directed events shown in Figure 5.12.

The general patterns are very similar to that of the northwest events albeit will opposed direction. Note the sediment transport fluxes are generally an order of magnitude smaller than during the northwest event, which is due to less energetic antecedent conditions that suspended less sediment.

For the different wave directions captured, the wave height increase due to relative focusing over the shallower disposal ground is directed more normally towards the Lyttelton Harbour entrance.

Net wave height increase remains small, representing only 3% increase relative to the existing bathymetry. The pattern of morphological changes over the event is clearly skewed to the southeast. Interestingly, as with the northwest event (Figure 5.11); the channel remains relatively protected from any sedimentation during this event (Figure 5.14).

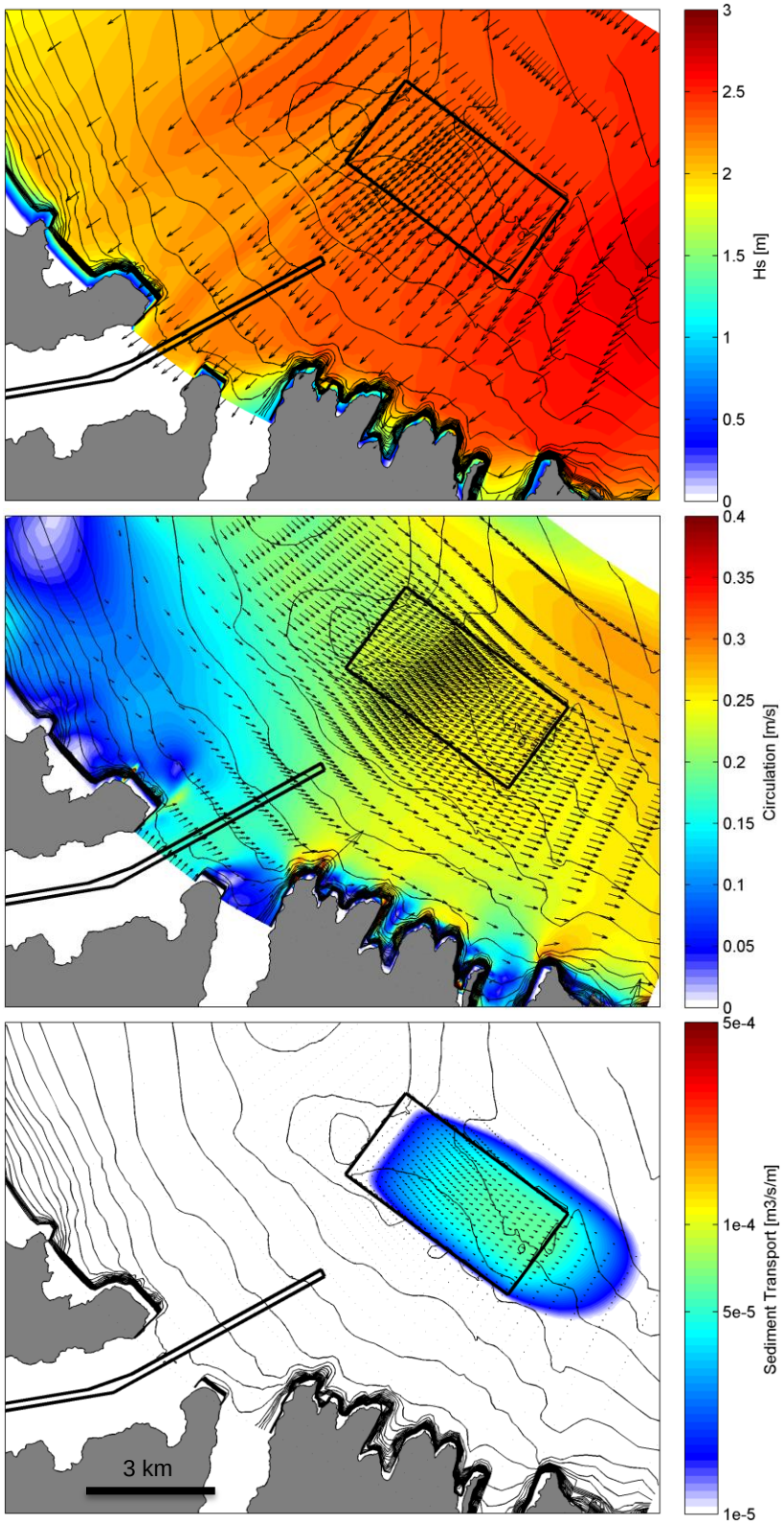


Figure 5.12 Wave, circulation and sediment transport field during southeast-directed residual currents over the post disposal bathymetry. Note a logarithmic colour scale is used for the sediment transport field.

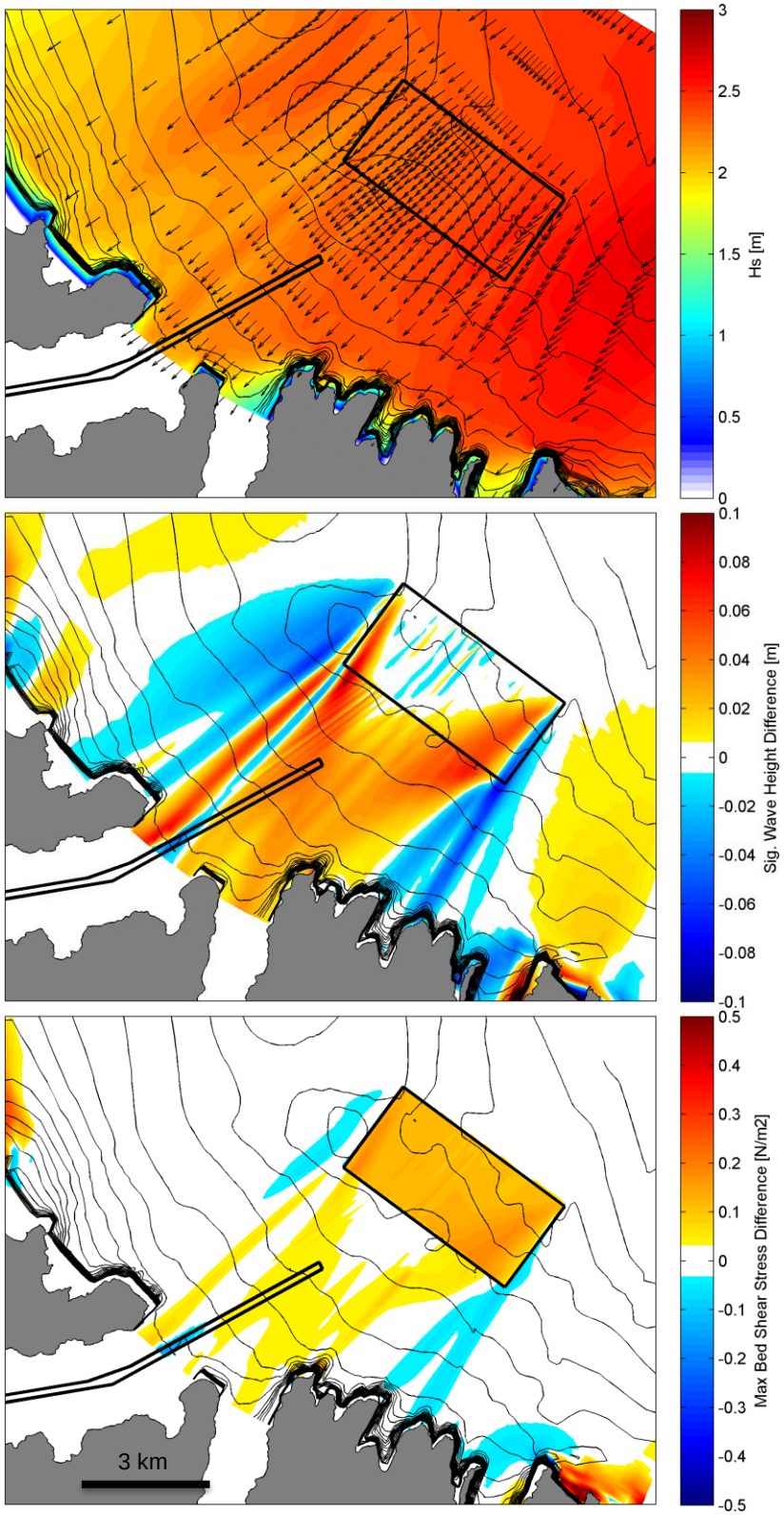


Figure 5.13 Significant wave height field over the post disposal bathymetry (top) and associated differences in significant wave height (middle) and maximum critical shear stress (bottom) relative to the existing state during the event with southeast -directed residual currents.

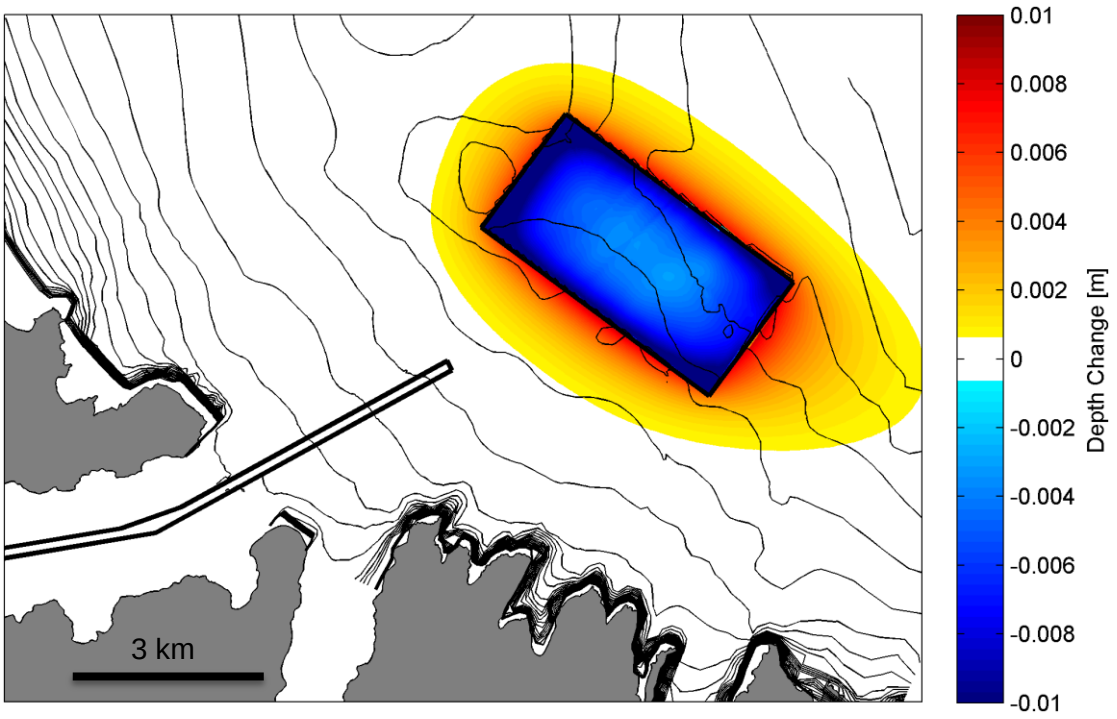


Figure 5.14 Morphological changes predicted at the end of the 4-day event with southeast - directed residual currents. A positive magnitude indicates sedimentation.

# 6. SUMMARY

Numerical modelling of the wave, hydrodynamic and sediment dynamics of an offshore disposal ground with bathymetry modified to include the disposal of 18 million cubic meters of (mostly cohesive) sediment has been undertaken. A suite of models has been employed, with detailed validation where possible. The results of the modelling are summarised as follows:

- A high resolution 10-year hindcast of the local wave climate was modelled using a three level nesting approach, starting from the New Zealand scale down to Pegasus Bay and Lyttelton Harbour. The offshore wave climate at the site is dominated by southerly swells, with less frequent, often locally generated, events from the easterly quadrant. At the proposed disposal site, this translates to a moderate-energy wave climate dominated by wave events from the east-northeast quadrant due to refraction effects around the Banks Peninsula, with a mean wave height of 0.9 m.

- A similar approach was employed to model a 10-year hindcast of the local tidal and residual hydrodynamics. At the proposed disposal site, the residual current regime is mostly bi-modal with either northwest of southeast-directed currents. The long term net residual is towards the southeast but of small net magnitude of ~1 $mm.s^{-1}$, indicating a relatively well balanced distribution of residual current events with opposing direction.

- The Delft3D modelling suite coupling high resolution, wave, flow and sediment transport models was applied to the study site to simulate the fate of cohesive sediment disposed within the proposed disposal ground. The models were nested within the calibrated wave and hydrodynamic regional models but no specific calibration of the sediment transport model could be performed due to lack of adequate field data. The modelling suite is therefore used as a tool to qualitatively investigate the key drivers and patterns of morphological changes at the disposal ground rather than produce quantitative predictions. Input reduction techniques were employed to simulate the morphological behaviour of the site, over both 1-year and 5-year periods. This was supplemented by simulation of real time events with high-energy wave forcing and large residual flow events with opposing direction (i.e. northwest and southeast directed).

- Morphodynamic simulations indicate that the disposed sediment will be mobilized throughout the proposed ground under the action of the combined tidal, residual, and wave forcing. Although simulations of discrete events indicate that the instantaneous sediment transport direction will depend on the ambient hydrodynamic forcing direction, the year-long simulations predict a net sediment spreading footprint consistently skewed towards the west. This westerly direction is consistent with the wave direction and suggests the wave action is the primary driver of morphological changes at the site, outweighing the residual and tidal current forcing effects.

- The relative depth increase throughout the ground due to the sediment disposal is expected to result in enhanced interaction with waves. Wave focusing developing over the shallower ground region can amplify the incident wave energy and redirects slightly elevated wave energy levels in the lee of the ground, including towards the Harbour entrance region. The elevated seabed level within the ground due to disposal is also expected to slightly increase the bed shear stress levels, thus enhancing the sediment transport potential.

- The year-long morphodynamic simulations undertaken in the present study suggest that the proposed new shipping channel position, although relatively close from the disposal ground, is not directly in the main path of net sediment migration from the ground that is primarily driven by wave action. However, the relative proximity means that slight modulations of the net transport direction due to inter-annual variability of the wave climate could still potentially expose the outer channel region to sedimentation from the disposal ground. Further, re-suspension of sediment dispersed from the ground is possible during energetic events; this suspended sediment load will be advected by the ambient currents and may be recirculated within the channel region but this is expected to be only a secondary sediment transport feature in terms of magnitude. Instantaneous morphological adjustments during events with strong northwest or southeast residual currents, which dominate the general hydrodynamic regime, results in sediment dispersion footprints skewed in the direction of the ambient residual flows, in an alongshore axis rather than directed onshore towards the channel.

# 7. REFERENCES

Brown, J.M., Davies A.G., 2009. Methods for Medium-term Prediction of the Net Sediment Transport by Waves and Currents in Complex Coastal Regions. Cont. Shelf Res. 29, 1502–1514.

Coastal Engineering Research Center, 1984. Shore Protection Manual. Coastal Engineering Research Center.

Collins, J., 1972. Prediction of Shallow Water Spectra. J. Geophys. Res. 77, 2693–2707.

Dastgheib, A., 2012. Long-term Process-based Morphological Modeling of Large Tidal Basins (Ph. D.). UNESCO-IHE.

De Vriend, H.J., Capobianco, M., Chesher, T., de Swart, H.J., Latteux, B., Stive, M.J.F., 1993. Approaches to long-term modelling of coastal morphology: a review. Coast. Eng. 21, 225–226.

Deltares, 2013. User Manual Delft3D-FLOW. version: 3.15.2789. Deltares.

Engelund, F., Hansen, E., 1967. A Monography on Sediment Transport in Alluvial Streams. Danish Technical ITeknisk Forlag).

Fredsøe, J., 1984. Turbulent Boundary Layer in Wave-current interaction. J. Hydraul. Eng. ASCE 110, 1103–1120.

Goring, D., 2009. Currents Outside Lyttelton Harbour: Analysis of ADP Data. Mulgor Consulting Ltd., Christchurch.

Grunnet, N. M., Walstra, D.J.R., Ruessink, B.G., 2004. Process-Based Modelling of a Shoreface Nourishment. Coast. Eng. 7, 581–607.

Haidvogel, D.B., Arango, H.G., Hedstrom, K., Beckmann, A., Malanotte-Rizzoli, P., Shchepetkin, A.F., 2000. Model Evaluation Experiments in the North Atlantic Basin: Simulations in Non-linear Terrain-Following Coordinates. Dyn. Atmosphere Oceans 32, 239–281.

Holthuijsen, L.H., 2007. Waves in oceanic and coastal waters. Cambridge University Press.

Latteux, B., 1995. Techniques for Long-term Morphological Simulation Under Tidal Action. Mar. Geol.

Lesser, G.R., 2009. An approach to medium-term coastal morphological modelling (Ph. D.). UNESCO-IHE & Delft Technical University.

Lesser, G.R., Stelling, G.S.,, Roelvink J.A., 2004. Development and Validation of a Three-Dimensional Morphological Model. Coast. Eng. 51, 883–915.

OCEL Consultant Limited, 2013. Deepening and Extension of the Navigation Channel – Capital and Maintenance Dredging, Impacts on the Physical Environment (Technical report prepared for Lyttelton Port of Christchurch). OCEL Consultant Limited.

Reniers, A.J.H.., Roelvink, J.A., Thornton, E.B., 2004. Morphodynamic Modeling of an Embayed Beach Under Wave Group Forcing. J. Geophys. Res. 109, 148–227.

Roelvink J.A., 2006. Coastal morphodynamic evolution techniques. Coast. Eng. 277–287.

Saha, S., Moorthi, S., Pan, H.-L., Wu, X., Wang, J., Nadiga, S., Tripp, P., Kistler, R., Woollen, J., Behringer, D., Liu, H., Stokes, D., Grumbine, R., Gayno, G., Wang, J., Hou, Y.-T., Chuang, H.-Y., Juang, H.-M.H., Sela, J., Iredell, M., Treadon, R., Kleist, D., Van Delst, P., Keyser, D., Derber, J., Ek, M., Meng, J., Wei, H., Yang, R., Lord, S., Van Den Dool, H., Kumar, A., Wang, W., Long, C., Chelliah, M., Xue, Y., Huang, B., Schemm, J.-K., Ebisuzaki, W., Lin, R., Xie, P., Chen, M., Zhou, S., Higgins, W., Zou, C.-Z., Liu, Q., Chen, Y., Han, Y., Cucurull, L., Reynolds, R.W., Rutledge, G., Goldberg, M., 2010. The NCEP Climate Forecast System Reanalysis. Bull. Am. Meteorol. Soc. 91, 1015–1057. doi:10.1175/2010BAMS3001.1

Sneddon, R., 2009. Assessment of Impacts to Benthic Ecology and Marine Ecological Resources from Proposed Capital Dredging and Spoil Disposal Offshore from Lyttelton Harbour (Technical report prepared for Lyttelton Port of Christchurch). Cawthron.

Tolman, H.L., 1991. A Third-Generation Model for Wind Waves on Slowly Varying, Un-steady and Inhomogeneous Depths and Currents. J. Phys. Oceanogr. 21, 782–797.

Van der Wegan, M., Roelvink, J.A., 2008. Long-term Morphodynamic Evolution of a Tidal Embayment using a Two-Dimensional, Process-based Model. J. Geophys. Res. 114.

Walstra, D.J.R., Hoekstra, R., Tonnon, P.K., Ruessink, B.G., 2013. Input reduction for long-term morphodynamic simulations in wave-dominated coastal settings. Coast. Eng. 77, 57–70. doi:http://dx.doi.org/10.1016/j.coastaleng.2013.02.001

Whitehouse R J S, Soulsby R L, Roberts W and Mitchener H J, 2000. The dynamics of estuarine muds, Thomas Telford Publications, London.